APL Photonics

Tutorial on optoelectronic oscillators

Cite as: APL Photonics **6**, 061101 (2021); https://doi.org/10.1063/5.0050311
Submitted: 14 March 2021 • Accepted: 25 May 2021 • Published Online: 15 June 2021

Ming Li, Tengfei Hao, Wei Li, et al.

Tutorial on optoelectronic oscillators

Cite as: APL Photon. 6, 061101 (2021); doi: 10.1063/5.0050311
Submitted: 14 March 2021 • Accepted: 25 May 2021 •
Published Online: 15 June 2021

Ming Li,[1,2,3,a] Tengfei Hao,[1,2,3] Wei Li,[1,2,3] and Yitang Dai[4]

AFFILIATIONS

[1] State Key Laboratory on Integrated Optoelectronics, Institute of Semiconductors, Chinese Academy of Sciences, Beijing 100083, China
[2] Center of Materials Science and Optoelectronics Engineering, University of Chinese Academy of Sciences, Beijing 100190, China
[3] School of Electronic, Electrical and Communication Engineering, University of Chinese Academy of Sciences, Beijing 100049, China
[4] State Key Laboratory of Information Photonics and Optical Communications, Beijing University of Posts and Telecommunications, Beijing 100876, China

[a] **Author to whom correspondence should be addressed:** ml@semi.ac.cn

ABSTRACT

Microwave photonic approaches for the generation of microwave signals have attracted substantial attention in recent years, thanks to the significant advantages brought by photonics technology, such as high frequency, large bandwidth, and immunity to electromagnetic interference. An optoelectronic oscillator (OEO) is a paradigmatic microwave photonic oscillator that produces microwave signals with ultra-low phase noise, thanks to the high-quality-factor of the OEO cavity that is achieved with the help of optical energy storage elements, such as low-loss optical fiber or a high-quality-factor optical resonator. Different OEO architectures have been proposed to generate spectrally pure single-frequency microwave signals with ultra-low phase noise. Multiple oscillation mode control methods have been proposed in recent years to obtain different kinds of microwave signals. With the rapid development of photonic integration technologies, prototypes of integrated OEOs have been demonstrated with compact size and low power consumption. Moreover, OEOs have also been used for sensing, computing, and signal processing. This Tutorial aims to provide a comprehensive introduction to the developments of OEOs. We first discuss the basic principle and the key phase noise property of OEOs and then focus on its developments in spectrally pure low phase noise signal generation and mode control methods, its chip-scale integration, and its applications in various fields.

I. INTRODUCTION

An optoelectronic oscillator (OEO) is a hybrid microwave and photonic system capable of producing self-sustained microwave oscillations when modulated light waves from a modulator fall on a photodetector. The output electrical signal of the photodetector (PD) is transmitted back to the modulator to form a closed optoelectronic feedback loop in the OEO cavity, and microwave oscillations arise from the noise when the loop gain exceeds the loss.[1–8] Early versions of OEOs can be dated back to 1968 in a study of mode-locked lasers,[9] where optoelectronic feedback loops were used to achieve stable mode-locking. Ten years later, the concept of an electro-optical oscillator was proposed by Kersten,[10] which was essentially an OEO. The feedback paths were relatively short in the early versions of OEOs. A conceptual breakthrough of the OEO was achieved by Yao and Maleki[1–4] by introducing a long low-loss fiber delay line as the energy storage element, which provided the most attractive high-quality-factor feature of modern OEOs. The authors analyzed in detail the operation of the long fiber-based oscillator and also introduced the acronym "OEO."

One of the key motivations of the studies of OEOs is the ultra-low phase noise resulting from the high-quality-factor of the OEO cavity, which is achieved by using high-quality-factor optical energy storage elements, such as low-loss optical fiber or a high-quality-factor optical resonator. High-frequency microwave signals can also be easily generated since the bandwidth of an OEO is only limited by the bandwidths of the optoelectronic devices in its cavity, which are as large as 100 GHz. These features are very attractive compared with its electrical counterparts, since the features may not be achievable in the electrical domain based on

traditional microwave resonator oscillators or systems that are costly and complicated.

In the past few decades, there has been an increasing effort in exploring OEOs in various fields. For example, several mode control and selection methods have been proposed and demonstrated to generate ultra-low phase noise single-frequency microwave signals and other complex microwave waveforms. Single-frequency microwave signals with low phase noise[11] can be generated in a single-loop OEO, where an electrical filter is used for mode selection. However, the spectral purity is limited since the bandwidth of the electrical filter is generally not narrow enough to select the desired oscillation mode. To overcome this problem, several OEO structures, such as dual-loop OEOs,[12–18] coupled OEOs (COEOs),[19–25] injection-locked dual-OEOs,[26–29] and parity-time (PT) symmetric OEOs,[30–41] have been proposed. The spectral purity can be enhanced even when an electrical filter with a relatively large bandwidth is used. The spectral purity can also be enhanced in a high-quality-factor optical resonator-based OEO,[5,6,42–45] since this resonator can be used to filter out undesired modes. Frequency tunable OEOs[45–61] have been proposed using frequency tunable electrical or microwave photonic filters (MPFs) to tune the center frequency of the generated single-frequency microwave signal. Frequency doubling and multiplying, as well as the generation of triangular waveforms, have also been demonstrated by manipulating the sidebands of the modulators.[62–74] Moreover, the generation of complex microwave signals, such as chirped microwave waveforms,[75–91] phase-locked stable single-mode and multi-mode signals,[92] broadband chaotic signals,[7,93–102] and random signals,[103] has also been demonstrated by properly controlling the cavity modes of OEOs. As a hybrid microwave photonic oscillator, OEOs have also been used for the generation of optical signals, such as optical pulses or frequency combs.[19–24,104–112] Although different kinds of microwave and optical signals can be generated using OEOs, most of the proposed systems were implemented based on discrete devices with a large size and high power consumption. Integrated OEOs[113–128] with compact size and low power consumption have been fabricated using indium phosphide (InP), silicon, and other platforms in recent years, which are key steps toward a new generation of compact microwave sources for demanding applications. In addition to signal generation, OEOs for other applications, such as sensing,[129–141] computing,[142–150] and signal processing,[90,91,151–175] have also been demonstrated, showing the great potential of OEOs in various applications. Since the basic principle and characteristics of OEOs have already been well summarized in other excellent literature,[5–8] we refer readers to these papers for a detailed overview. In this Tutorial, we first discuss briefly the basic principle and the phase noise property of OEOs and then focus on a comprehensive introduction to its developments in the past few decades.

The outline of this paper is as follows: In Sec. II, we provide the basic operation principle and phase noise of an OEO. In Sec. III, we provide examples to generate spectrally pure low phase noise microwave signals using different OEO architectures, including dual-loop OEO, COEO, OEO based on a high-Q ring resonator, and PT-symmetric OEO. Oscillation mode control methods to produce tunable single-frequency microwave signals, as well as other complex microwave signals, are described in Sec. IV. We investigate methods such as frequency tuning using tunable filters, chirped signal generation using Fourier domain mode-locking, stable multi-mode oscillation based on a nonlinear parametric process, complex oscillation based on nonlinear dynamics, and random oscillation based on random scattering. In Sec. V, we discuss recent advances in integrated OEOs that have compact size and low power consumption. Sec. VI provides an overview of OEO applications, including sensing, computing, and signal processing. We conclude this Tutorial in Sec. VII.

II. OPERATION PRINCIPLE AND PHASE NOISE OF AN OEO

A. Basics of OEO cavity modes

An OEO is a hybrid resonant oscillator that consists of an optical part and an electrical part to form a closed optoelectronic feedback loop. The schematic diagram of a typical single-loop OEO using a narrowband electrical filter is shown in Fig. 1. An electrical signal in the electrical part is modulated onto an optical carrier from a laser source using an electro-optic modulator (EOM), and the modulated optical signal in the optical part is converted back to an electrical signal at a PD. Generally, a narrowband filter is used for mode selection, and an optical fiber is adopted to ensure low phase noise. An optical amplifier, such as an erbium-doped fiber amplifier (EDFA) or/and an electrical amplifier (EA), can be used to provide enough gain for the oscillating signal in the OEO loop. Once the cavity gain exceeds the loss, self-sustained oscillation is established directly from noise.

Several models[2,3,93,176] have been introduced to analyze the OEO operation in the past few decades. For example, the model proposed by Yao and Maleki[2,3] is one of the most well-known models to analyze the steady-state single-mode oscillation of OEOs. This model is based on the quasi-linear theory. The propagation of the oscillating signal is analyzed after one cavity round-trip, and the final steady-state of the oscillating signal is obtained by a regenerative feedback approach. A comprehensive simulation model to calculate the features of OEO dynamics was been proposed by Levy *et al.*[176] by generalizing the Yao–Maleki model and including

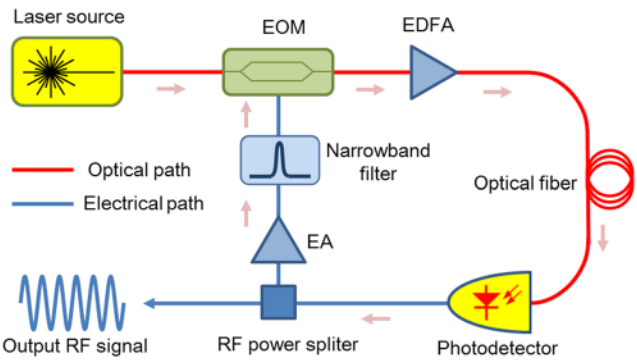

FIG. 1. Schematic diagram of a typical single-loop OEO. A closed optoelectronic feedback loop is formed in the OEO cavity. Generally, a narrowband filter is used for mode selection. Self-sustained oscillation can be established from noise once the gain exceeds the loss. EOM, electro-optic modulator; EDFA, erbium-doped fiber amplifier; and EA, electrical amplifier.

other required physical effects, such as the mode competition effect in the OEO cavity, the fast response time of the EO modulator, and the fluctuations of the output signal. Moreover, a model based on the delay-differential equation (DDE)[93] was introduced to analyze the nonlinear dynamics of OEOs; this model will be discussed in Sec. IV D.

Here, we use the Yao–Maleki model as an example to analyze the OEO operation. In this model, the oscillation signal of the OEO is linearized if a loop filter with a narrow enough bandwidth is used to block all harmonic frequency components. Specifically, we assume that the electrical signal $V_{in}(t)$ applied to the EOM is a sinusoidal wave, i.e., $V_{in}(t) = V_0 \sin(\omega t + \beta)$, where V_0, ω, and β are the amplitude, angular frequency, and initial phase, respectively, of the electrical signal. Then, the output signal $V_{out}(t)$ of the EA can be expressed as

$$\begin{aligned} V_{out}(t) &= V_{ph}\left\{1 - \eta \sin\pi\left[\frac{V_{in}(t)}{V_\pi} + \frac{V_B}{V_\pi}\right]\right\} \\ &= \left\{V_{ph}1 - \eta\ \sin\left(\frac{\pi V_B}{V_\pi}\right)\left[J_0\left(\frac{\pi V_0}{V_\pi}\right) + 2\sum_{m=1}^{\infty} J_{2m}\right.\right. \\ &\quad \left.\times \left(\frac{\pi V_0}{V_\pi}\right)\cos(2m\omega t + 2m\beta)\right] + 2\eta\ \cos\left(\frac{\pi V_B}{V_\pi}\right) \\ &\quad \left.\times \sum_{m=0}^{\infty} J_{2m+1}\left(\frac{\pi V_0}{V_\pi}\right)\sin[(2m+1)\omega t + (2m+1)\beta]\right\}, \quad (1) \end{aligned}$$

where $V_{ph} = I_{ph}RG_A$ is the photovoltage at the output of the EA. $I_{ph} = \rho\alpha P_0/2$ is the photocurrent generated at the output of the PD, and R, ρ, and P_0 are the load impedance, responsivity, and input power of the PD, respectively. G_A is the voltage gain of the EA, α is the insertion loss of the EOM, and η determines the extinction ratio of the EOM by ER = $(1+\eta)/(1-\eta)$. V_π and V_B are the half-wave voltage and bias voltage of the EOM, respectively. J_n is the n-th order Bessel function of the first kind.

As can been seen from Eq. (1), the output signal $V_{out}(t)$ contains many harmonic frequency components of ω. If the bandwidth of the loop filter is narrow enough to block all harmonic frequency components, $V_{out}(t)$ can be linearized as

$$V_{out}(t) = G(V_0)V_{in}(t), \quad (2)$$

where $G(V_0)$ is the voltage-gain coefficient, which can be expressed as

$$G(V_0) = G_S\frac{2V_\pi}{\pi V_0}J_1\left(\frac{\pi V_0}{V_\pi}\right), \quad (3)$$

where G_S is the small signal gain of the OEO loop, which is defined as

$$G_S = \left.\frac{dV_{out}}{dV_{in}}\right|_{V_{in}=0} = -\frac{\eta\pi V_{ph}}{V_\pi}\cos\left(\frac{\pi V_B}{V_\pi}\right). \quad (4)$$

As can be seen from Eqs. (3) and (4), the voltage-gain coefficient $G(V_0)$ is related to V_{ph} and V_π, which are both a function of the frequency of the electrical signal. A unitless complex filter function $\tilde{F}(\omega)$ is introduced to account for all the frequency-dependent components in the loop; thus, the voltage-gain coefficient $G(V_0)$ can be treated as a frequency independent term. The unitless complex filter function can be expressed as

$$\tilde{F}(\omega) = F(\omega)\exp[i\phi(\omega)], \quad (5)$$

where $F(\omega)$ is the normalized transmission function and $\phi(\omega)$ is the phase caused by the dispersive component in the OEO cavity. In this way, the electrical signal after one cavity round-trip of the OEO can be expressed as

$$\tilde{V}_{out}(t) = \tilde{F}(\omega)G(V_0)\tilde{V}_{in}(\omega, t), \quad (6)$$

where $\tilde{V}_{out}(t)$ and $\tilde{V}_{in}(t)$ are the complex output and input signal of the OEO, respectively.

If the OEO loop is closed, self-sustained oscillation can be established from noise. According to Eq. (6), the recurrence relationship for a single-frequency component $\tilde{V}_{in}(\omega, t) = \tilde{V}_{in}(\omega)\exp(i\omega t)$ of the noise spectrum can be written as

$$\tilde{V}_n(\omega, t) = \tilde{F}(\omega)G(V_0)\tilde{V}_{n-1}(\omega, t - T'), \quad (7)$$

where n is the number of cavity round-trip times and T' is the time delay caused by the physical length of the OEO loop. The initial noise component is amplified in the OEO loop after each cavity round-trip while its gain is gradually decreased. A stable oscillation can be achieved when the gain is equal to unity. According to the principle of superposition, the stable output signal of the OEO can be calculated as the summation of all circulating fields, which can be expressed as

$$\begin{aligned} \tilde{V}(\omega, \mathrm{t}) &= G_A\tilde{V}_{in}(\omega)\sum_{n=0}^{\infty}\tilde{F}(\omega)G(V_0)\exp\left[i\omega\left(t - nT'\right)\right] \\ &= \frac{G_A\tilde{V}_{in}\ \exp(i\omega t)}{1 - \tilde{F}(\omega)G(V_0)\exp(i\omega T')}. \end{aligned} \quad (8)$$

The stable output power can therefore be expressed as

$$\begin{aligned} \mathrm{P}(\omega) &= \frac{|\tilde{V}(\omega, \mathrm{t})|^2}{2R} \\ &= \frac{\frac{G_A^2|\tilde{V}(\omega)|^2}{2R}}{1 + |\mathrm{F}(\omega)\mathrm{G}(V_0)|^2 - 2F(\omega)|\mathrm{G}(V_0)|\cos[\omega T' + \phi(\omega) + \phi_0]}, \end{aligned} \quad (9)$$

where ϕ_0 is related to the sign of $\mathrm{G}(V_0)$. As can be seen from Eq. (9), only a number of frequency-periodic modes can be coherently summed and can exist in the OEO cavity. The frequencies of these cavity modes are determined by

$$\omega T' + \phi(\omega) + \phi_0 = 2k\pi, \quad k = 0, 1, 2\ldots, \quad (10)$$

where k is the mode number. The frequency spacing between adjacent cavity modes can be written as

$$\mathrm{FSR} = 1/T, \quad (11)$$

where $T = T' + \left.\frac{d\phi(\omega)}{d\omega}\right|_{\omega=\omega_{osc}}$ is the total loop delay of the OEO loop, including the physical length delay and the dispersion-induced group delay. Generally, the dispersion-induced delay can be considered constant for different cavity modes when the optical fiber is not

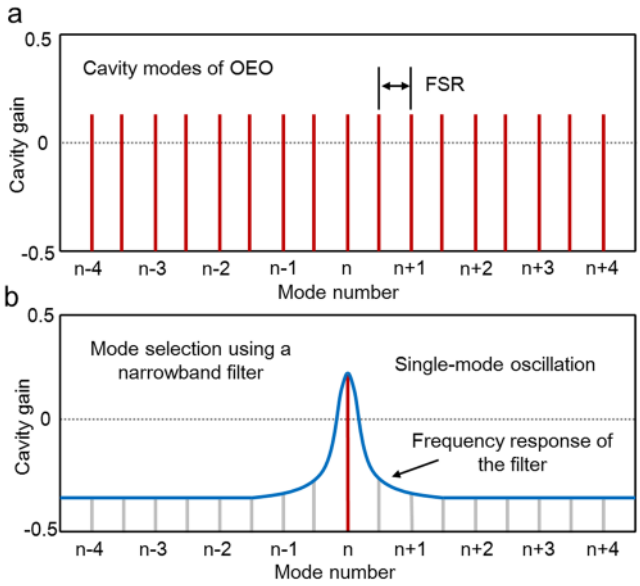

FIG. 2. Cavity modes and single-mode selection in an OEO. (a) Potential cavity modes of a filter-free single-loop OEO. The frequency of the cavity modes can be expressed as k × FSR, where k is an integer and FSR is the free spectral range of the OEO. (b) Single-mode oscillation can be achieved by using a narrowband filter to select one of the cavity modes.

very long. As shown in Fig. 2(a), the frequency of the cavity modes can be expressed as k × FSR when $\phi_0 = 0$; thus, there are lots of closely distributed potential oscillation modes. A narrowband filter is required to select one of the cavity modes and achieve single-mode oscillation, which is shown in Fig. 2(b).

B. Basics of the phase noise of an OEO

Ultra-low phase noise is one of the most attractive features of an OEO. For any real oscillator that is able to produce a specific single-frequency signal, its frequency fluctuates from an ideal sine wave. The phase noise of an oscillator reflects its short-term frequency stability, which is related to the frequency fluctuation that occurs over a short period of seconds or less. As shown in Fig. 3, the phase noise is defined as the ratio of the noise power in a 1 Hz bandwidth at a certain offset frequency to the signal power at the center frequency, which is measured in dBc/Hz. Generally, the phase noise of an oscillator is characterized as the single-sideband (SSB) phase noise, where the phase noise is plotted as a function of the offset frequency.

The phase noise is very important in modern radar, communication, and other applications since the calibration algorithms in these applications can only be used to improve the long-term frequency stability, and generally, it is the short-term frequency stability that determines the performance of these systems. For example, the OEO can be served as a local oscillator (LO) in radar and communication systems. In radar systems, the low phase noise is a crucial requirement of the LO; otherwise, the target echo signal will be submerged in noise and cannot be detected.[7,177] In communication systems, a detection error may occur because

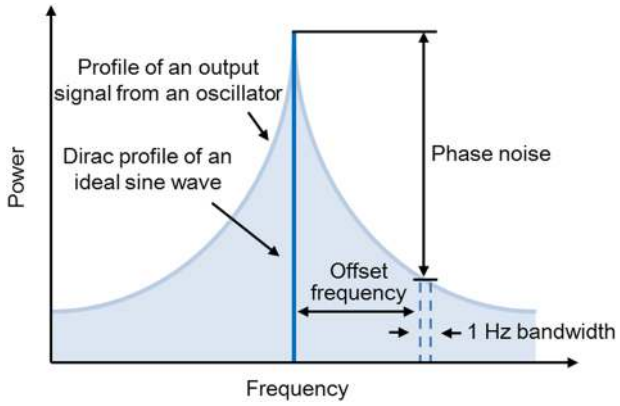

FIG. 3. Sketch map of the phase noise of an oscillator. The output signal of a real oscillator fluctuates from an ideal sine wave. The phase noise of an oscillator is defined as the ratio of the noise power in a 1 Hz bandwidth at a certain frequency offset to the signal power at the center frequency, which is measured in dBc/Hz.

signal constellation rotation and intercarrier interference are caused by the phase noise of the LO;[178] thus, low phase noise is very important.

The phase noise characteristic of the OEO can be approximated by the power spectral density because it is equal to the sum of the SSB phase-noise density and the SSB amplitude-noise density, and the latter is much lower than the former in most cases.[2,3] According to the Yao–Maleki model, the power spectral density of the OEO is calculated as[2,3]

$$S_{RF}(f') = \frac{\delta}{(2-\delta/T) + 2\sqrt{1-\delta/T}\cos(2\pi T f')}, \tag{12}$$

where f' is the offset frequency from the oscillation mode, $\delta = \rho_N G_A^2 / P_{osc}$ is defined as the input noise-to-signal ratio of the oscillator, $\rho_N = \left|\tilde{V}_{in}(\omega)\right|^2 / 2R\Delta f$ is the equivalent input noise density of the oscillator, and Δf is the frequency bandwidth. In the case of $2\pi T f' \ll 1$, the power spectral density of the OEO can be further simplified as

$$S_{RF}(f') = \frac{\delta}{(\delta/2T)^2 + (2\pi T f')^2}. \tag{13}$$

In the OEO loop, the input noise density ρ_N consists of the thermal noise density of the amplifier $\rho_{thermal} = 4k_B T_e(NF)$, the shot noise density of the PD $\rho_{shot} = 2eI_{ph}R$, and the relative intensity noise (RIN) density of the laser $\rho_{RIN} = N_{RIN} I_{ph}^2 R$, which can be written as

$$\rho_N = 4k_B T_e(NF) + 2eI_{ph}R + N_{RIN} I_{ph}^2 R, \tag{14}$$

where k_B is the Boltzmann constant, T_e is the room temperature, NF is the noise figure of the amplifier, e is the electron charge, and N_{RIN} is the RIN of the laser source.

As can be seen from Eq. (13), the power spectral density or the SSB phase noise of OEO decreases quadratically with the total loop delay T. By using optical fiber with a low insertion loss of about 0.2 dB/km as the energy storage element, a large T of tens of or even hundreds of μs can be achieved, which is one of the

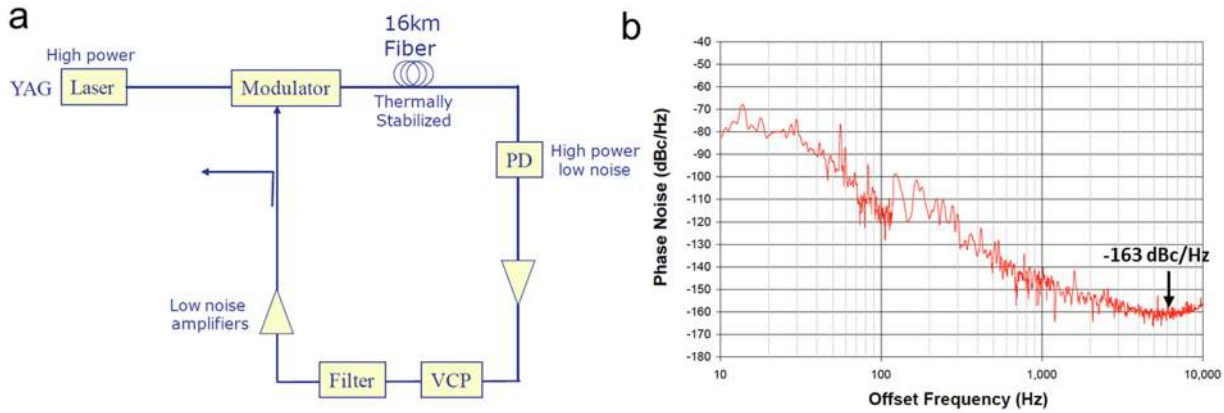

FIG. 4. A single-loop OEO with ultra-low phase noise. (a) Schematic diagram of the low phase noise OEO. (b) Measured phase noise performance. VCP: voltage controlled phase shifter. Figures from D. Eliyahu, D. Seidel, and L. Maleki, *IEEE International Frequency Control Symposium*. Copyright 2008 IEEE. Reproduced with permission from IEEE.

most important features of OEO and results in low phase noise. Equation (13) also indicates that the phase noise can be reduced by raising the oscillation power for a fixed ρ_N and G_A; thus, low phase noise can be achieved by using a laser source with high output power and a PD with high power handling capability. At the same time, the lowest achievable phase noise is limited by the loop residual phase noise of the active devices in the OEO cavity, such as the thermal noise of the amplifier, the shot noise of the PD, and the RIN of the laser. As a result, a large loop delay, high oscillation power, and low-noise active devices should be adopted to ensure ultra-low phase noise.

As shown in Fig. 4, a single-loop 10 GHz OEO with ultra-low phase noise was designed in Ref. 11. A 16-km long optical fiber, a high-power Yttrium Aluminum Garnet (YAG) laser, a high-power low-noise PD, and two low-noise amplifiers were adopted. A low phase noise of −163 dBc/Hz at 6 kHz offset frequency was achieved, representing an OEO architecture with the lowest measured phase noise.

It is also necessary to compare the phase noise performance of OEOs and electrical oscillators. Electrical oscillators are one of the most commonly used oscillators in different science and technology fields. Low-noise microwave signals at low center frequencies can be easily obtained using electrical quartz and dielectric resonator-based oscillators with low cost, compact size, and a simple structure. However, the generation of high-frequency microwave signals with low phase noise is challenging. Generally, high-frequency microwave signals are obtained by multiplying low-frequency signals generated by high-performance electrical oscillators, but the phase noise is also degraded by $20 \times \log N$ in the frequency multiplication process, where N is the multiplication factor. In contrast, an OEO can produce high-frequency microwave signals with ultra-low phase noise, thanks to the use of a low-loss optical delay line or high-quality-factor optical resonator. Indeed, the lowest phase noise of 10 GHz microwave oscillators is achieved using the above-mentioned OEO in Ref. 11. Nevertheless, most of the existing OEOs are based on discrete optoelectronic devices, which have a large size and high power consumption.

III. OEO ARCHITECTURES FOR SPECTRALLY PURE HIGHLY STABLE MICROWAVE SIGNAL GENERATION

As mentioned above, an OEO with low phase noise can be achieved using a long optical fiber as the loop delay line. However, the long optical fiber also results in a small free spectral range (FSR), increasing the difficulty of single-mode selection. For instance, the FSR of the ultra-low phase noise OEO reported in Ref. 11 is about 12.8 kHz. Ideally, a loop filter with 3-dB bandwidth lower than 12.8 kHz should be used for single-mode selection, but this filter is hard to achieve, especially at high center frequencies. For example, a high-quality electrical filter centered at 10 GHz only has a 3-dB bandwidth of 10 MHz.[179] The use of a loop filter with a wide bandwidth results in undesirable side modes, and the spectral purity of the generated signal deteriorates. In practical radar systems, the sideband mode-induced spurs may cause false alarm; thus, it should be suppressed to reduce the false alarm probability. To overcome this problem, schemes such as dual-loop OEO, COEO, OEO with high-Q resonators, and PT-symmetric OEO have been proposed, where spectrally pure low phase noise microwave signals can be obtained. In addition to methods that optimize the short-term frequency stability, i.e., the phase noise, several techniques have also been proposed and demonstrated to improve the long-term frequency stability of OEO. These methods are also important for real-world applications.

A. Dual-loop OEO

One of the most commonly adopted structures to overcome the trade-off between low phase noise and single-mode selection is the dual-loop OEO.[12] In this OEO, the equivalent FSR is increased using the Vernier effect. Figure 5 shows the schematic diagram and single-mode selection in a typical dual-loop OEO. The optical signal is divided into two parts by an optical coupler, and the two parts are combined in the electrical domain using a RF power combiner; thus, a dual-loop structure is constructed. Optical fibers with different lengths are used in the two loops, respectively. According to Eq. (11), the two loops have different FSRs due to their different

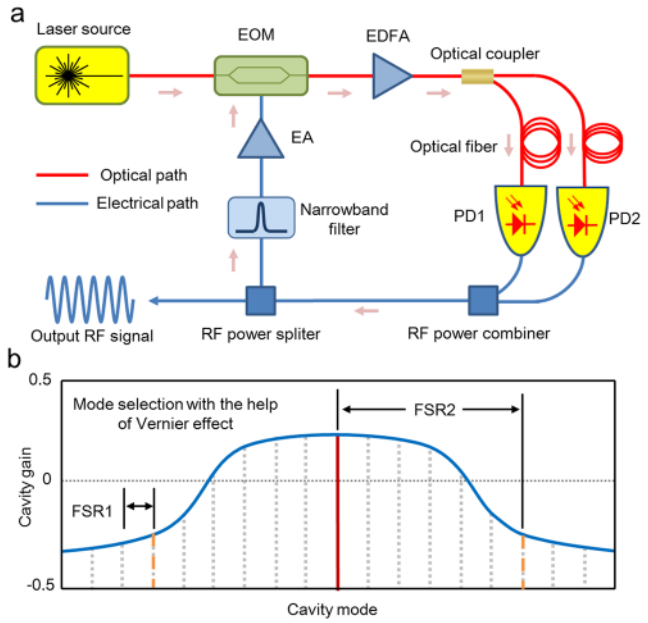

FIG. 5. Schematic diagram and single-mode selection in a typical dual-loop OEO. (a) A dual-loop structure is achieved by dividing the OEO loop into two parts using optical coupler and combining the two parts by using a RF power combiner. (b) The FSRs of the two loops are different due to the different loop lengths. Only the cavity modes with frequencies of f = m ×FSR1 = n × FSR2 can oscillate, where m and n are integers and FSR1 and FSR2 are the FSR of the two loops, respectively.

optical fiber lengths, since the FSR of the OEO loop is determined by the loop delay. As shown in Fig. 5(b), an equivalent narrowband filter is obtained based on the two different FSRs due to the Vernier effect. The frequency of the oscillation modes of the dual-loop OEO is defined as follows:

$$f = m \times \mathrm{FSR1} = n \times \mathrm{FSR2}, \tag{15}$$

where m and n are integers and FSR1 and FSR2 are the FSRs of the two loops, respectively. In this case, the equivalent mode spacing of the dual-loop OEO is enlarged, thanks to the Vernier effect; thus, single-mode oscillation with high spectral purity can be achieved even by using a loop filter with relatively large bandwidth.

In addition to the configuration shown in Fig. 5(a), several other configurations have been proposed and demonstrated to construct dual-loop OEOs, for example, by combining the two loops in the optical domain using polarization multiplexing[13] or wavelength multiplexing.[14] Moreover, multi-loop structures[15–18] with more than two loops have also been implemented to obtain high-purity microwave signals with low supermode noise. At the same time, the overall Q-factor of the dual-loop or multi-loop OEO is lower than that of the single-loop OEO using the same length of long optical fiber; thus, the phase noise is increased.

B. COEO

It is possible to reduce the optical fiber length in the OEO cavity while maintaining a high Q-factor by using the COEO consisting of an optical loop and an optoelectronic loop.[19–25] Figure 6(a) shows a typical schematic diagram of the COEO. A ring laser is constructed in the optical loop using an optical filter, amplifier, and fiber. The generated light wave from the ring laser is coupled to the optoelectronic loop using an EOM, which is shared by the two loops. The optoelectronic loop in Fig. 6(a) is an OEO, whose optical pump is generated by the ring laser. An RF filter with narrow passband is used for mode selection in the optoelectronic loop; thus, an RF signal can be generated. If the frequency of the generated RF signal is integer multiples of the FSR of the ring laser, active mode-locking of the laser can be achieved by feeding the obtained RF signal to the EOM, since the intensity of the optical field of the ring laser is modulated by the RF signal. In the COEO, the Q-factor is multiplied by the active nature of the optical OEO; thus, lower phase noise can be achieved compared with a conventional OEO using the same optical fiber length. In addition, the unwanted side modes can also be eliminated with a commonly available electrical filter due to the wide FSR of the optoelectronic loop resulting from the short delay.

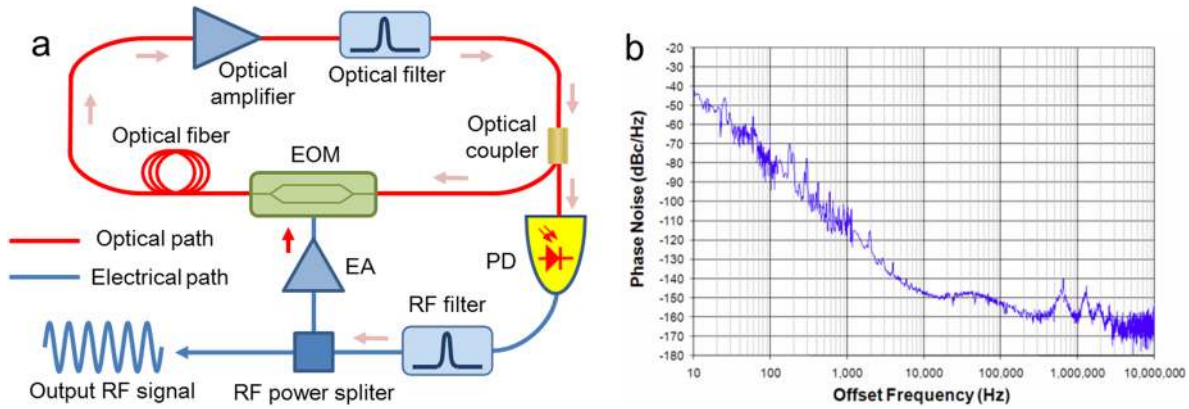

FIG. 6. A coupled OEO. (a) Schematic diagram of the coupled OEO. (b) Measured SSB phase noise of the generated 10-GHz microwave signal. Ultra-low phase noise of −148 dBc/Hz at 10 kHz offset frequency is achieved. Panel (b) is from D. Eliyahu, D. Seidel, and L. Maleki, *IEEE International Frequency Control Symposium*. Copyright 2008 IEEE. Reproduced with permission from IEEE.

The measured phase noise of the COEO using a 140-m fiber is shown in Fig. 6(b). An ultra-low phase noise of −148 dBc/Hz at 10 kHz offset frequency is achieved.[11] It would require a much longer fiber length to achieve similar performance for a conventional OEO. In addition to the generation of single-frequency microwave signals, a train of optical pulses and frequency combs can also be generated in the ring laser cavity of the COEO since the ring laser is an active mode-locked laser. In addition, the use of a shorter fiber length has added benefits, such as compact size and lower sensitivity to environmental perturbations. It should be noted that similar configurations consisting of an optical part and an electrical part were developed in the late 1960s,[9] when an optoelectronic feedback loop was used to study the mode-locking of lasers.

C. OEO based on a high-Q resonators

Another solution to overcome the trade-off between low phase noise and single-mode selection in fiber-based OEOs is using a high-Q resonator instead of optical fiber as the energy storage element. Figure 7(a) shows the schematic diagram of a the high-Q resonator-based OEO.[5,6,42–45] The high-Q resonator serves as a filter to remove the unwanted modes and as a modulator in the OEO loop. Generally, a whispering gallery-mode resonator (WGMR) fabricated from optically transparent materials, such as lithium tantalate and lithium niobate, serves as the high-Q resonator, with a Q-factor as high as 3×10^{11}. The bandwidth associated with this large Q-factor is narrow enough to filter out the unwanted side modes. In addition, the Q-factor of the OEO loop is enhanced by the high-Q property of the resonator, since the Q-factor of the OEO loop is related to the Q-factor of its optoelectronic components. As a result, low phase noise can be ensured by using the high-Q resonator.

The WGMRs also have a very small size, ranging from several hundreds of micrometers to few millimeters. WGMR-based OEOs have a very small size making them highly desirable in advanced applications requiring a high-performance microwave source with compact size and low phase noise. Moreover, the output frequency of the WGMR-based OEOs can be tailored in the range of 10–40 GHz or higher, which is determined by the FSR of the WGMR. The phase noise and photograph of a packaged 30 GHz lithium niobate WGMR-based OEO are shown in Fig. 7(b), As can be seen, the measured phase noise is about −110 dBc/Hz at 10 kHz offset frequency for the generated 30 GHz signal. The size of the packaged OEO is as small as a coin; thus the WGMR-based OEO has a high performance and compact size.

D. Parity-time symmetric OEO

In recent years, PT-symmetry has been used in OEOs as a novel mode selection approach; stable single-mode oscillation can be achieved without using narrowband electrical or optical filters.[30,31] The right part of Fig. 8(a) shows the schematic diagram of a typical PT-symmetric OEO. The PT-symmetric OEO has two coupled loops with identical loop length. By precisely manipulating the relationship between gain and loss in the two loops to satisfy the PT-symmetry condition, i.e., the gain of one loop is balanced by the loss of another loop, the losses overcompensate the gain for all cavity modes, except for the one with the highest gain. As a result, single-mode oscillation can be achieved in the cavity mode with the highest gain. Low phase noise can also be achieved since a spool of long optical fiber or a high-Q resonator can also be used. It should be noted that spectrally pure single-mode oscillation can be obtained in the PT-symmetric OEO with a small cavity FSR. This is a unique and attractive feature of the PT-symmetric OEO, since the effective cavity FSR is indeed enlarged to achieve spectrally pure single-mode oscillation in the dual-loop OEO, COEO, and resonator-based OEO.

The dynamic equations of the nth cavity mode in the two coupled loops are as follows:

$$\frac{da_n^{(1)}}{dt} = \left(i\Delta\omega_n^{(1)} + g\right)a_n^{(1)} - i\mu a_n^{(2)}, \tag{16}$$

$$\frac{da_n^{(2)}}{dt} = \left(i\Delta\omega_n^{(2)} - \gamma\right)a_n^{(2)} - i\mu a_n^{(1)}, \tag{17}$$

where $a_n^{(1)}$ and $a_n^{(2)}$ are the amplitudes of the nth cavity mode in the gain and loss loops, respectively. i is the imaginary unit. $\Delta\omega_n^{(1,2)} = \omega_n - \omega_n^{(1,2)}$ is the detuning frequency of the two loops. ω_n is the

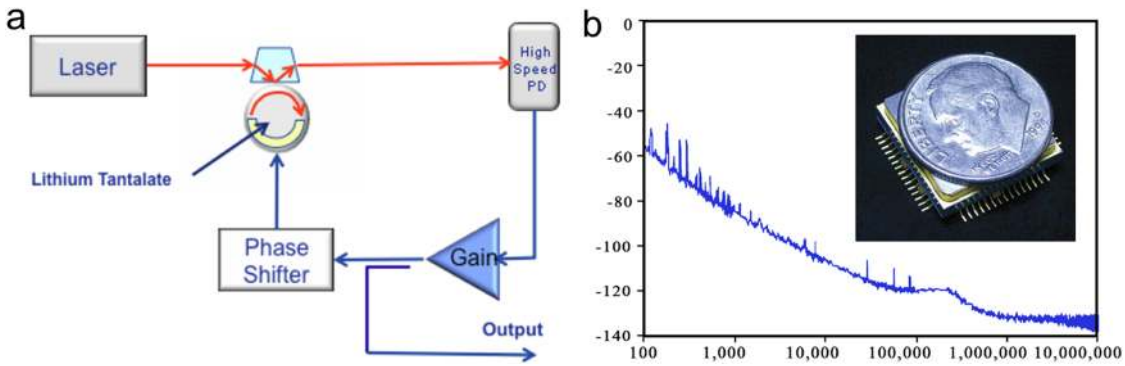

FIG. 7. An OEO based on a high-Q resonator. (a) Schematic diagram. A high-Q resonator is used to store the energy of the OEO. (b) Measured phase noise performance. Inset shows the photograph of a packaged OEO based on a lithium niobate WGMR. Panel (a) is from L. Maleki, *European Frequency and Time Forum*. Copyright 2012 IEEE. Reproduced with permission IEEE. Panel (b) is reproduced with permission from L. Maleki, Nat. Photonics **5**, 728–730 (2011). Copyright 2011 Nature Publishing Group.

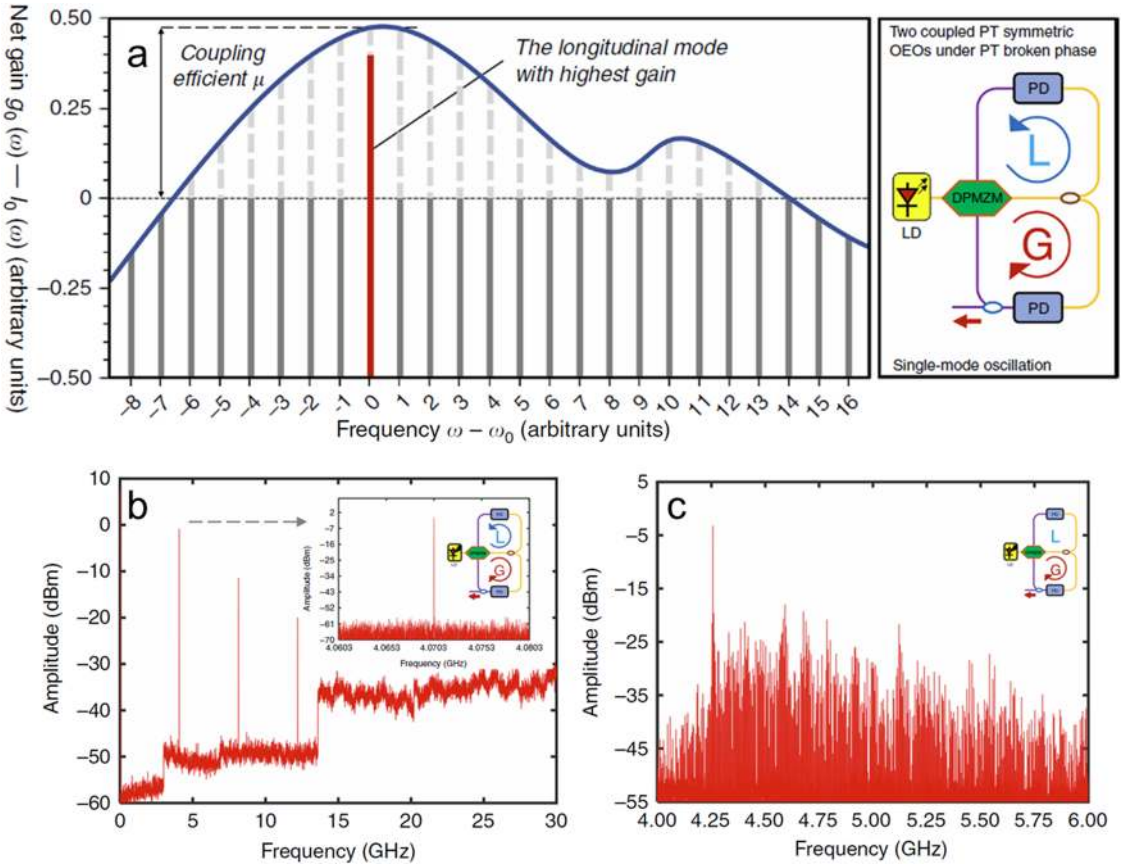

FIG. 8. Mode selection and single-mode oscillation in a PT-symmetric OEO. (a) PT-symmetric phase of the OEO with two coupled loops. The gain of one loop is balanced by the loss of another loop, and the losses overcompensate the gain for all cavity modes, except for the one with the highest gain. Single-mode oscillation can be achieved in the cavity mode with the highest gain. (b) Measured spectrum of the single-mode oscillation. (c) Measured multi-mode spectrum without PT-symmetry. Figures reproduced with permission from Liu *et al.*, Light: Sci. Appl. **7**(1), 38 (2018). Copyright 2018 Author(s), licensed under a Creative Commons Attribution 4.0 License.

angular frequency of the nth cavity mode, and $\omega_n^{(1,2)}$ are the eigenfrequencies of the two loops. μ is the coupling coefficient between the two loops. g and γ are the gain and loss coefficients of the gain and loss loops, respectively. By solving Eqs. (16) and (17), we can obtain the eigenfrequencies of the supermodes of the PT-symmetric system,

$$\omega_{n\pm} = \frac{\omega_n^{(1)} + \omega_n^{(2)}}{2} + \frac{i(g-\gamma)}{2} \pm \sqrt{\mu^2 - \left(\frac{g+\gamma}{2} - \frac{i\left(\omega_n^{(1)} - \omega_n^{(2)}\right)}{2}\right)^2}. \quad (18)$$

If the loop lengths of the two loops are the same, we have $\omega_n^{(1)} = \omega_n^{(2)}$. If the PT-symmetry condition can be satisfied by precisely manipulating the gain and loss in the two loops, i.e., $g = \gamma$, Eq. (18) can be further rewritten as

$$\omega_{n\pm} = \omega_n \pm \sqrt{\mu^2 - \gamma^2}. \quad (19)$$

Equation (19) indicates a transition point in the PT-symmetric system when the gain/loss coefficient is equal to the coupling coefficient μ. If the gain/loss coefficient is larger than the coupling coefficient, PT-symmetry no longer applies, and the frequency difference of the eigenfrequencies of the supermodes becomes imaginary. Thus, a pair of amplifying and decaying modes is generated in each loop with identical frequencies. As a result, single-mode oscillation can be achieved in the gain loop. Otherwise, the two loops oscillate at two slightly different frequencies if the gain/loss coefficient is smaller than the coupling coefficient, since the eigenfrequencies of the supermodes are split into two slightly different frequencies.

Figure 8(b) shows the measured single-mode oscillation spectrum of the PT-symmetric OEO in the experiment. The gain and loss of the two loops are precisely tuned to the same magnitude of the oscillating signal to satisfy the PT-symmetry condition. It should be noted that the OEO would oscillate in multimode without PT-symmetry. Figure 8(c) shows the measured multimode oscillation spectrum without PT-symmetry.

In addition to the frequency-fixed PT-symmetric OEO in Refs. 30–33, frequency tunable PT-symmetric OEOs have also been

proposed and demonstrated in recent years using a tunable filter in the OEO loop.[34–41] In these methods, coarse frequency selection with a certain tuning range is achieved by changing the center frequency of the loop filter. Fine-frequency selection is subsequently achieved using PT-symmetry.

E. Long-term frequency stability of OEO

Although the above-mentioned OEOs have excellent phase noise performance at high offset frequencies, the phase noise at low offset frequencies is generally poor because of the fact that the free-running OEOs are sensitive to environmental perturbations, such as temperature fluctuations and vibrations. For example, a typical temperature coefficient of the single-mode fiber in the OEO cavity is 34 ps/km/°C. The stability of a 1-km fiber-based OEO would be deteriorated by a delay change of 34 ps if the temperature is changed by 1°. The unwanted environmental perturbations also deteriorate the long-term frequency stability of OEOs, which is critical for real-world applications. Several techniques have been proposed to solve this problem, such as temperature-insensitive fiber,[180] thermal stabilization,[181] injection locking,[26–29] and phase locking.[2,182–186] Injection locking is a simple and effective frequency stabilization method to synchronize the OEO to a reference source by injecting the reference signal into the OEO loop; however, the phase noise performance of the injection-locked OEO is limited by the reference source. Phase locking is another frequency stabilization method to lock the OEO to a reference source using a phase-locked loop (PLL), which can substantially improve the long-term frequency stability while maintaining low phase noise. An example of a frequency-stabilized OEO using PLL is shown in Fig. 9(a). The output signal of the dual-loop OEO is compared to the reference source using a phase-frequency detector (PFD) after frequency division, and the filtered feedback signal of the PFD is sent to the OEO to shift the phase of the microwave signal for frequency

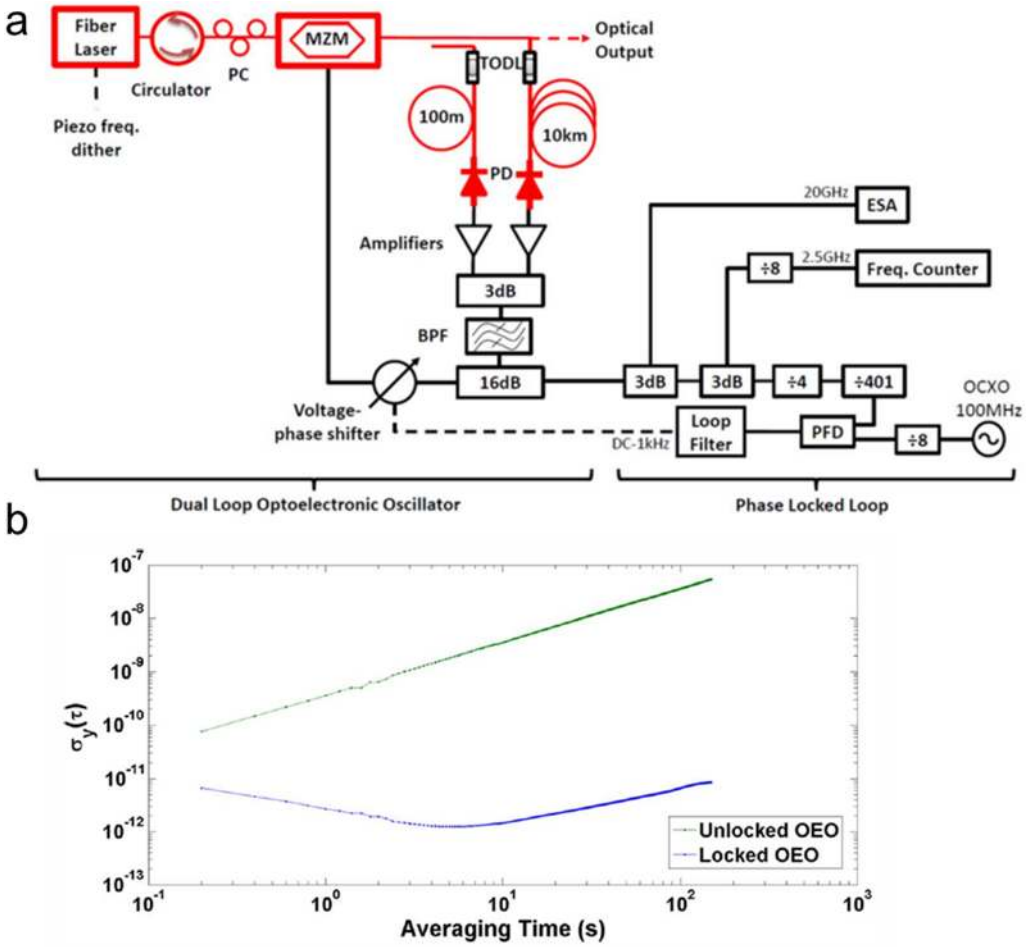

FIG. 9. A frequency-stabilized OEO using a phase-locked loop. (a) Schematic diagram. The output signal of the dual-loop OEO is divided into a low-frequency signal and compared to the reference source using a phase-frequency detector (PFD). The filtered feedback signal is sent to the OEO to shift the phase of the microwave signal using a voltage phase shifter. (b) Overlapping Allan deviation (ADEV) of the OEO before and after phase locking. Figures reproduced with permission from Bluestone *et al.*, IEEE Trans. Microwave Theory Tech. **63**, 1046 (2015). Copyright 2015 IEEE.

TABLE I. Performance of selected key OEO architectures for low phase noise microwave signal generation.

Architecture	Frequency (GHz)	Phase noise (dBc/Hz)	References
Single-loop OEO	10	−163 (@ 6 kHz)	11
Dual-loop OEO	10	−140 (@ 10 kHz)	12
COEO	10	−148 (@ 10 kHz)	11
WGMR-based OEO	30	−110 (@ 10 kHz)	5
PT-symmetric OEO	4	−139 (@ 10 kHz)	30
Phase-locked OEO	10	−139 (@ 10 kHz)	186

stabilization. Figure 9(b) shows the measured Allan deviation (ADEV) of the OEO. The long-term frequency stability is significantly improved after phase locking.

The key OEO architectures and their phase performances for low phase noise microwave signal generation are summarized in Table I.

IV. OSCILLATION MODE CONTROL OF OEO

An OEO has a multimode cavity, and the frequency of each cavity mode is an integral multiple of the FSR. As a result, various microwave signals, such as tunable single-frequency microwave signals, chirped microwave signals, and other complex microwave waveforms, can be obtained from an OEO cavity with appropriate control of the OEO oscillation modes. In this section, several OEO oscillation mode control methods are discussed, including schemes based on frequency tunable filtering, Fourier domain mode-locking, the optoelectronic parametric process, nonlinear dynamics, and randomly distributed feedback.

A. Wideband frequency tunable OEO

Frequency tunable microwave sources are highly desired in practical applications, since the working frequency of the whole system can be tuned to achieve the best system performance with the help of the tunable microwave sources. Generally, a narrowband electrical filter is used in the OEO loop to select the desired single-frequency oscillation mode. The passband of the narrowband electrical filter is usually fixed; thus, the frequency tunability of the OEO is limited. The use of a tunable electrical filter or electrical filter bank, as well as a tunable microwave photonic filter (MPF), has been proposed and demonstrated to obtain frequency tunable OEOs.[45–61] For example, a magnetically tunable yttrium-iron-garnet (YIG) filter was used in Ref. 46, achieving a wide frequency tuning range of tens of gigahertz. The disadvantage of the YIG filter is that the unwanted fluctuation of the magnetic field results in the center frequency fluctuation of the filter, leading to a frequency change in the generated microwave signal. This problem can be solved by replacing the YIG filter with a tunable MPF. The MPF can be implemented using various schemes, such as using a sliced broadband optical source, multitap structure, phase modulation to intensity modulation (PM-IM) using stimulated Brillouin scattering (SBS), or phase-shifted fiber Bragg grating (PS-FBG).[48–61] Similar to an electrical filter, the MPF can be considered as a two-port system with an electrical input port and an electrical output port. Inside the MPF, the input electrical signal is first up-converted to the optical domain with the help of an EOM, and then it is processed and filtered by optical devices within the MPF. The output electrical signal is finally obtained by down-converting the filtered signal at a PD. Frequency tuning of the MPF can be achieved by tuning the property of its optical devices.

Figure 10 shows the schematic diagram and spectra of the generated microwave signals of a wideband tunable OEO based on PM-IM conversion using SBS.[57] As can be seen, two lasers are used: one is the signal laser and the other is the pump laser. The light wave from the signal laser is sent to the phase modulator (PM), and the pump wave is injected into the high nonlinear fiber (HNLF) to enable SBS. The +1st and −1st sidebands of the output phase-modulated light wave of the PM have the same magnitude but the opposite phase; thus, the beat between the signal wave and the two sidebands is canceled out if the phase-modulated light wave is sent directly to the PD. The SBS in this scheme ensures that one of the 1st sidebands is amplified by the backscattered Stokes wave, changing the balance of the two 1st sidebands. As a result, an oscillating microwave signal can be obtained as the output of the PD as the beat note between the signal wave and the amplified sideband. The frequency of the oscillating microwave signal can be expressed as[57]

$$\nu_{osc} = |\nu_0 - \nu_p + \nu_B|, \tag{20}$$

where ν_0 and ν_p are the frequencies of the signal and pump laser, respectively, and ν_B is the Brillouin frequency shift of SBS. As can be seen from Eq. (20), the oscillation frequency can be tuned by tuning the frequency of the signal or pump laser, achieving frequency tunability. In the experiment, a widely tunable range from DC to 60 GHz is achieved; the range is only limited by the bandwidth of the optoelectronic components in the OEO loop.

B. Fourier domain mode-locked OEO

In addition to the generation of single-frequency microwave signals, another very attractive direction of OEOs is the generation of chirped microwave waveforms with fast frequency scanning, providing a wide range of applications in radar and communication systems. For example, chirped microwave waveforms can be used in modern radar systems to increase the range resolution while maintaining a large detection distance, which overcomes the long-existing trade-off between the range resolution and detection distance in a traditional radar system. Chirped microwave waveforms with tunable parameters have been generated using tunable OEOs in Refs. 187 and 188. However, the OEO produces single-frequency signals and the chirped microwave waveforms are generated at the outside of the OEO cavity using a baseband electrical chirped microwave source or a recirculating phase modulation loop.

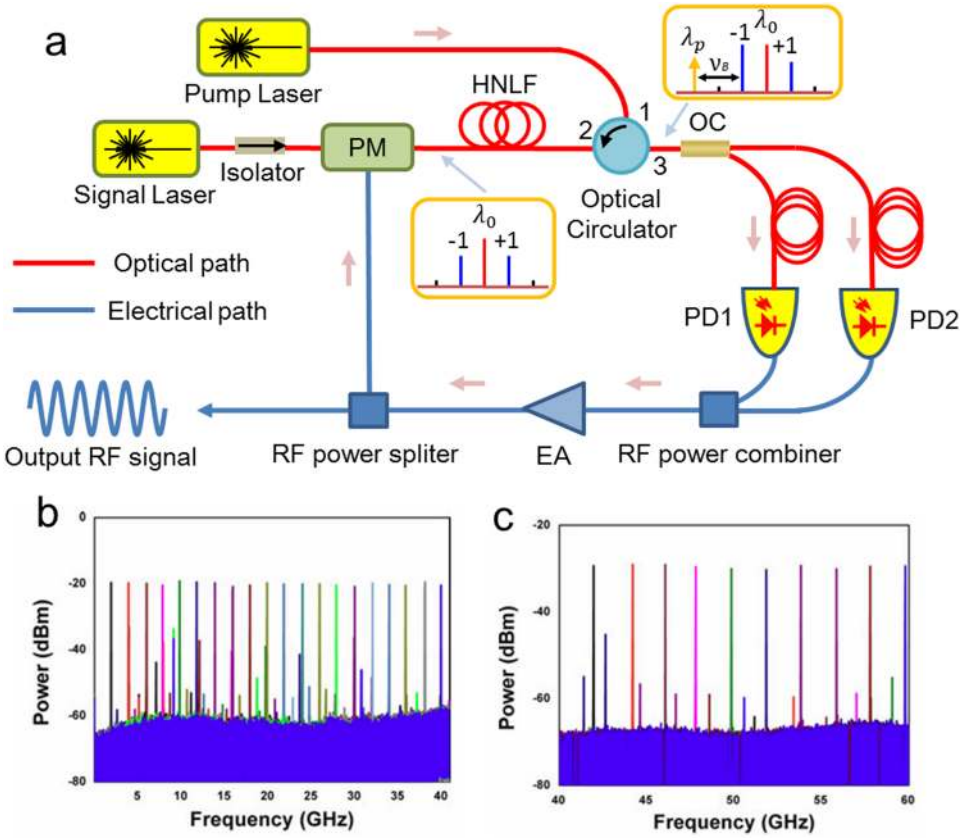

FIG. 10. A frequency tunable OEO using a tunable microwave photonic filter based on stimulated Brillouin scattering (SBS). (a) Schematic diagram. (b) and (c) Electrical spectra of the generated microwave signal with a tunable frequency range of up to 60 GHz. PM, phase modulator; HNLF, high nonlinear fiber; OC, optical coupler; PD, photodetector; and EA, electrical amplifier. Panels (b) and (c) are reproduced with permission from Peng *et al.*, J. Lightwave Technol. **33**(13), 2707–2715 (2015). Copyright 2015 IEEE.

Recently, we proposed and demonstrated an OEO cavity mode control method based on Fourier domain mode-locking.[75] Chirped microwave waveforms were generated directly from the OEO cavity. Figures 11(a) and 11(b) shows a comparison of a traditional single-frequency OEO and the Fourier domain mode-locked OEO (FDML OEO). A single passband filter is incorporated in the traditional OEO cavity, and the output signal is a single-frequency sinusoidal wave. In the FDML OEO cavity, a frequency scanning filter is used. The scanning period of the filter is synchronized with the cavity round-trip time of the OEO to enable the Fourier domain mode-locking operation, i.e.,

$$T_{\text{roundtrip}} = \text{n} \times T_{\text{filter drive}}, \tag{21}$$

where $T_{\text{filter drive}}$ is the cavity round-trip time, $T_{\text{filter drive}}$ is the scanning period of the filter, and n is an integer. By doing so, the frequency scanning filter is tuned at the same spectral position when the selected mode returns to this position after one cavity round-trip time. For example, the frequency of the selected cavity modes would also be f_1 and f_2 at $t_1 + T_{\text{roundtrip}}$ and $t_2 + T_{\text{roundtrip}}$, respectively, if the frequency of the selected cavity modes is f_1 and f_2 at t_1 and t_2, respectively. As a result, all the cavity modes can be stored and activated simultaneously in the OEO cavity and are mode-locked with fixed phase relationship if their frequencies are within the frequency scanning range of the filter. The synchronization between the tuning period and the cavity round-trip time in FDML OEO is similar with that of synchronization in traditional active or passive mode-locking, except that the mode-locking is achieved in the frequency domain in the FDML OEO. The output signal of the FDML OEO is a frequency scanning/chirped microwave waveform due to the frequency domain mode-locking.

Figure 11(c) shows the experimental setup of the FDML OEO. A frequency scanning MPF based on PM-IM conversion is used. The MPF consists of a frequency scanning laser diode, a PM, and an optical notch filter. The operation principle of the MPF is similar to that of the SBS-based tunable OEO in Fig. 10. In this scheme, the balance of phase modulation is interrupted by the optical notch filter. The center frequency of the MPF is equal to the frequency difference between the laser diode and the optical notch filter. By sweeping the frequency of the laser diode, a frequency scanning MPF can be achieved. In theory, the output signal of the MPF can be considered as the mixing product of the optical carrier and the to-be-blocked component of the MPF,[75] which can be expressed as

$$V_{\text{OUT}}^{\Omega}(t) = S\left(\left|V_{\text{IN}}^{\Omega}\right|\right)\left\{\left[V_{\text{IN}}^{\Omega}(t)e^{i\varphi_{\text{oc}}(t)}\right] * s_{21}^{\text{open loop}}(t)\right\}e^{-i\varphi_{\text{oc}}(t)} + n_A(t), \tag{22}$$

where $V_{\text{OUT}}^{\Omega}(t)e^{i\Omega t}$ and $V_{\text{IN}}^{\Omega}(t)e^{i\Omega t}$ are the output and input microwave signals of the MPF, respectively, and Ω is the center frequency of the microwave signal. $n_A(t)$ is the additive and intensity noise in the OEO. $S\left(\left|V_{\text{FDML}}^{\Omega}\right|\right)$ is the saturation factor of the PM-IM

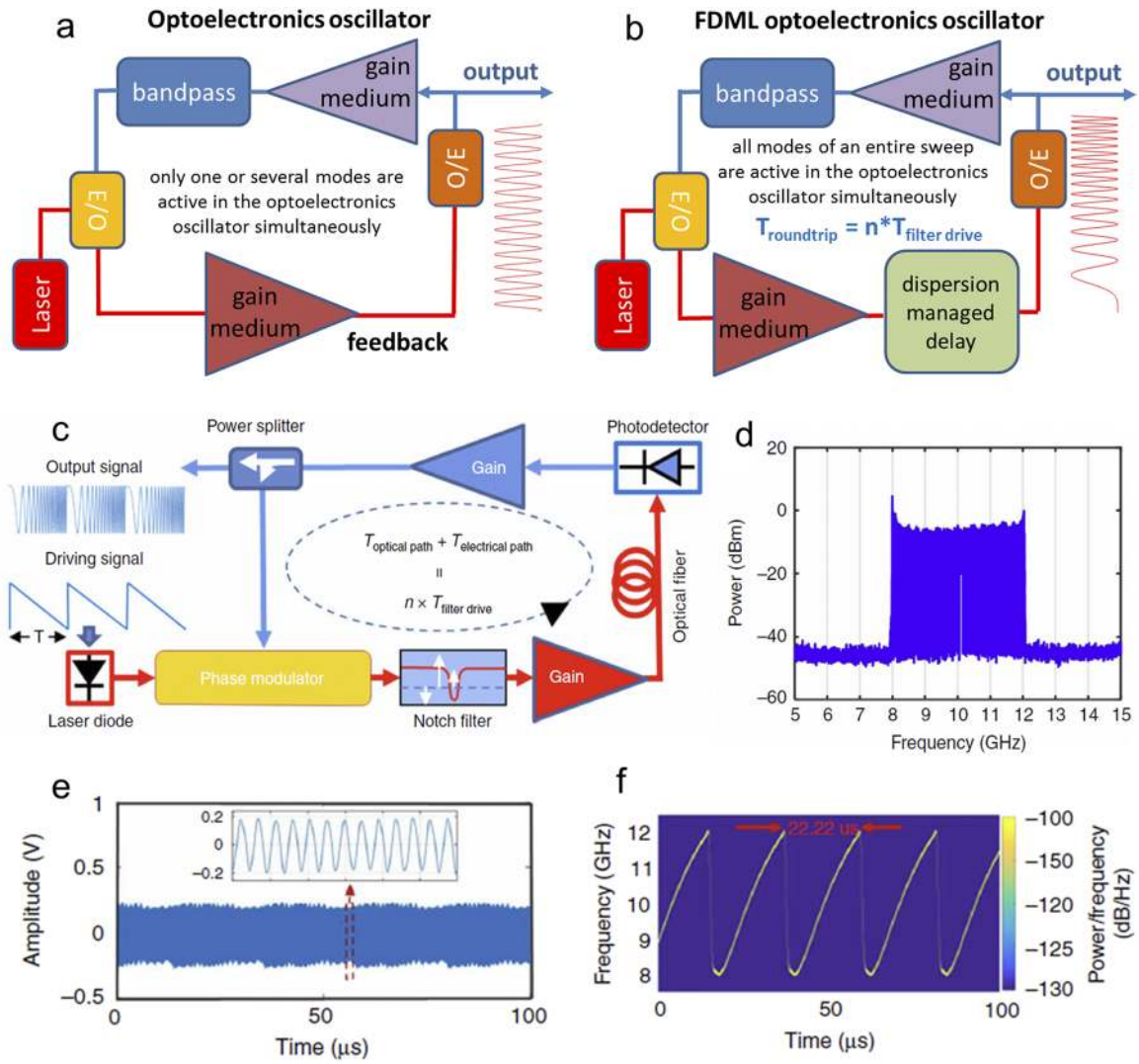

FIG. 11. Fourier domain mode-locked (FDML) OEO. (a) and (b) Comparison of a traditional single-frequency OEO and a FDML OEO. A single passband filter is incorporated in the traditional OEO, and the output is a sinusoidal wave. In the FDML OEO, a frequency scanning filter is used. The scanning period of the filter is synchronized with the cavity round-trip time to enable the Fourier domain mode-locking operation. The output is a frequency scanning/chirped microwave waveform. (c) Experimental setup. The frequency scanning microwave photonic filter consists of a frequency scanning laser diode, a phase modulator, and an optical notch filter. (d) Spectrum, (e) temporal waveform, and (f) instantaneous frequency–time of the output signal of the FDML OEO. Figures reproduced with permission from from Hao *et al.*, Nat. Commun. **9**, 1839 (2018). Copyright 2018 Author(s), licensed under a Creative Commons Attribution 4.0 License.

conversion process, and $s_{21}^{\text{open loop}}$ is the open-loop response of the OEO when the MPF is not scanning.

If the system noise is ignored, the frequency scanning oscillation in the OEO loop in the Fourier domain mode-locking operation should satisfy

$$V_{\text{FDML}}^{\Omega}\left(t - \text{T}_{\text{round-trip}}\right) = S\left(\left|V_{\text{FDML}}^{\Omega}\right|\right)\left\{\left[V_{\text{FDML}}^{\Omega}(t)e^{i\varphi_{\text{oc}}^{\text{T}_{\text{round-trip}}}(t)}\right] * s_{21}^{\text{open loop}}(t)\right\} \times e^{-i\varphi_{\text{oc}}^{\text{T}_{\text{round-trip}}}(t)}, \quad (23)$$

where $\varphi_{\text{oc}}^{\text{T}_{\text{round-trip}}}$ is the periodic phase variation of the laser diode in the Fourier domain mode-locking operation. Equation (23) indicates that the stable frequency scanning oscillation repeats itself after each cavity round-trip time. The solution of Eq. (23) can be expressed as

$$\text{V}_{\text{FDML}}^{\Omega}(\text{t}) \propto \text{e}^{-i\varphi_{\text{oc}}^{\text{T}_{\text{round-trip}}}}. \quad (24)$$

The frequency of the generated stable frequency scanning oscillation in the FDML OEO cavity follows the periodic frequency variation of the MPF since the center frequency of the MPF is determined by the frequency of the laser diode. It should be noted that in

addition to the PM-IM conversion-based MPF, other kinds of filters can also be used in the FDML OEO for mode selection,[87] as long as the center frequency of the filter can be rapidly tuned to ensure the Fourier domain mode-locking operation. In the Fourier domain mode-locking operation, chirped microwave signals can be generated directly from the FDML OEO cavity, and the frequency scanning parameters are determined by using the loop filter.

The spectrum, temporal waveform, and instantaneous frequency–time of the generated X-band (8–12 GHz) linearly chirped microwave waveform (LCMW) are shown in Figs. 11(d)–11(f). The frequency of the generated LCMW ranges from about 8 to 12 GHz, which can be easily tuned by changing the frequency scanning characteristics of the loop filter. The generated LCMW is constant in the time domain, indicating a good mode-locking state. The instantaneous frequency of the generated LCMW increases nearly linearly within one period. The frequency scanning period can also be tuned, for example, by changing the cavity length of the OEO or by harmonic mode-locking.[78] In addition to the LCMW, other kinds of chirped microwave waveforms have also been generated using an FDML OEO, such as dual-chirp microwave waveform,[80] a complementary LCMW pair,[81] phase coded microwave waveform,[82] phase-coded LCMW,[83] and frequency-doubled LCMW.[84] Moreover, a microwave photonic radar based on the FDML OEO has also been proposed and experimentally demonstrated,[89] which shows the great potential of FDML OEO in practical applications.

C. Mode control based on parametric frequency conversion process

As shown in Fig. 2(a), the cavity modes in a traditional OEO are discrete, and the minimum mode spacing is determined by the cavity delay T. This oscillator is called a delay-controlled oscillator, whose stable oscillating signal must repeat itself after one cavity round-trip time, if the timing jitter is ignored. As a result, the frequency of the output signal of a traditional OEO is constrained by the cavity delay T. The frequency must be n/T, where n is an integer. The delay-controlled operation leads to difficulty in frequency tuning. Frequency tuning is discrete unless a phase shifter is used to tune the cavity delay. Moreover, the initial phases of the cavity modes are not determined, and the mode competition effective is inevitable in a traditional delay-controlled OEO; thus, stable multimode oscillation is not possible if no mode-locking operation is applied. Recently, we proposed and experimentally demonstrated a phase-controlled optoelectronic parametric oscillator (OEPO)[92] based on parametric frequency conversion in the optoelectronic cavity, whose stable oscillation is not limited by the cavity delay.

The schematic diagram of the OEPO is shown in Fig. 12(a). The major difference between the OEPO and a traditional OEO is that an electrical nonlinear medium (electrical mixer) is introduced into the optoelectronic cavity for the parametric frequency conversion process. The electrical mixer is a nonlinear electrical device that produces new frequencies. The output frequency at the IF port of the mixer is equal to the difference between the two input frequencies at the LO and RF ports. As shown in Fig. 12(b), by applying a local oscillator at the LO port, a pair of oscillation modes are converted into each other by the local oscillator; thus, each mode repeats itself after two cavity round-trip times. More importantly, the sum phase of each mode pair is locked, and a phase jump of the oscillating signals occurs in the electrical nonlinear medium, leading to unique mode properties of the OEPO. For example, stable multimode oscillation can be easily achieved in the OEPO since the sum phase of each mode pair is locked. Stable multimode oscillation is difficult to achieve in a traditional OEO due to the unavoidable mode competition effect.

Mathematically, the stable oscillating mode pair in the OEPO should satisfy the following equations:

$$\begin{cases} s(z=0,t) = \alpha_1 p(z=L,t) s^*(z=L,t) + c.c., & (25a) \\ s(z=L,t) = \alpha_2 s(z=0,t+T) + n_a(t) + c.c., & (25b) \end{cases}$$

where $s(z,t) = e^{-i(\omega_{s1}t - k_{s1}z + \varphi_{s1})} + e^{-i(\omega_{s2}t - k_{s2}z + \varphi_{s2})} + c.c.$ is the oscillating mode pair; ω_{s1}, φ_{s1}, and k_{s1} are the angular frequency, initial phase, and wave vector of one mode, respectively; and ω_{s2}, φ_{s2}, and k_{s2} are those of another mode, respectively. z is the spatial position along the OEPO cavity, $z = 0$ denotes the position where the parametric frequency conversion is implemented, and L is the cavity length of the OEPO. α_1 is the frequency conversion loss, α_2 includes all the losses/gains when the oscillating mode pair travels from the output of the mixer to the input via the OEPO cavity, and $\alpha_1\alpha_1$ is the total loop gain. $p(z=0,t) = p(z=L,t) = e^{-i\omega_{lo}t} + c.c.$ is the pump signal from the local oscillator, and $\omega_{lo} = \omega_{s1} + \omega_{s2}$ is the angular frequency of the local oscillator. Equation (25a) describes the parametric frequency conversion, and Eq. (25b) shows that the stable oscillating mode pair recovers itself after one cavity round-trip T. In a stable oscillation, the total loop gain $\alpha_1\alpha_1$ is near unity, and the system noise $n_a(t)$ is generally negligible. According to Eq. (25), we can derive the following equation describing the angular frequencies and initial phases of the two modes:[92]

$$\begin{cases} \omega_{s1}, \omega_{s2} = \dfrac{\omega_{lo} \pm 2N\pi \times FSR}{2}, \\ \varphi_{s1} + \varphi_{s2} = \dfrac{-\omega_{lo}T + 2\mathrm{M}\pi}{2}, \end{cases} \quad (26)$$

where ω_{s1} and φ_{s1} are the angular frequency and initial phase of one mode, respectively, and ω_{s2} and φ_{s2} are those of another mode, respectively. $\omega_{lo} = \omega_{s1} + \omega_{s2}$ is the angular frequency of the local oscillator, and M and N are integers. As can be seen from Eq. (26), the frequency of the cavity modes of the OEPO is determined by the cavity delay and the local oscillator. The frequencies of each mode pair are symmetrical about half of the frequency of the local oscillator. The minimum mode spacing between the adjacent cavity modes is FSR/2, which is only half of that of a traditional OEO. Moreover, the sum phase of each mode pair is locked to $(-\omega_{lo}T + 2\mathrm{M}\pi)/2$, which is a unique phase-controlled operation.

Degenerate oscillation can be further achieved when the frequencies of the two modes in a mode pair are the same, i.e., $\omega_{s1} = \omega_{s2}$. According to Eq. (26), the frequency ω_s and initial phase φ_s of the degenerate oscillation can be expressed as

$$\begin{cases} \omega_s = \dfrac{\omega_{lo}}{2}, \\ \varphi_s = -\dfrac{\omega_s T}{2} + K\pi, \end{cases} \quad (27)$$

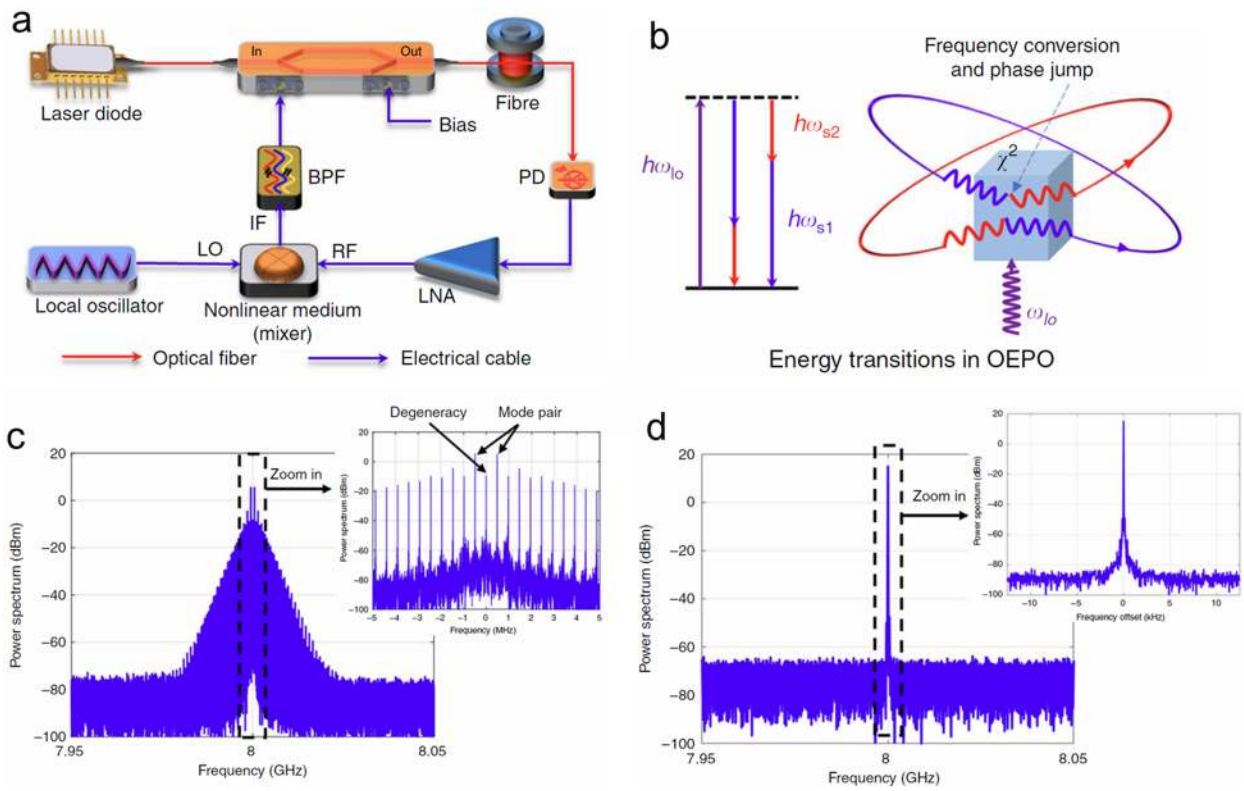

FIG. 12. An optoelectronic parametric oscillator (OEPO) that controls the cavity modes based on the optoelectronic parametric process. (a) Schematic diagram of the OEPO. An electrical mixer is introduced into the optoelectronic cavity as the nonlinear medium for the parametric process. (b) Energy transitions in the OEPO. A pair of cavity modes are converted into each other by a local oscillator in the electrical nonlinear medium, locking the sum phase of the mode pair, thanks to the phase jump in the frequency conversion process. (c) Spectrum of the generated stable multi-mode oscillation. (d) Spectrum of the generated single-mode oscillation. Figures reproduced with permission from Hao *et al.*Light: Sci. Appl. **9**, 102 (2020). Copyright 2020 Author(s), licensed under a Creative Commons Attribution 4.0 License.

where K is an integer. In this case, the oscillating signal is a single-frequency microwave signal whose frequency is free from the cavity delay. The initial phase of the degenerate oscillation is also locked to $-\omega_s T/2 + K\pi$. Due to this phase locking, i.e., the phase-controlled operation, cavity delay-independent frequency tuning can be achieved,[92] which is also not possible in a traditional OEO if the effective cavity delay is not tuned.

The measured multimode and single-mode spectra of the OEPO are shown in Figs. 12(c) and 12(d). The frequency of the local oscillator in our experiment is 16 GHz, and the FSR of the OEPO cavity is 1 MHz. We can see that the oscillating modes of the multi-mode oscillation are symmetrical about half of the frequency of the local oscillator and the minimum mode spacing is FSR/2, which is consistent with our theory. The multimode oscillation is stable in our experiment once the OEPO is switched on, thanks to the fact that the sum phase of each mode pair of OEPO is locked, whereas the multimode oscillation in a traditional OEO is not stable due to the random initial phases of each mode. Degenerate single-mode oscillation is achieved in our experiment by using a loop filter with a narrow enough bandwidth. A frequency tuning step of 100 Hz is also achieved in our experiment,[92] which is much less than the 1-MHz cavity FSR of the OEPO.

In addition to microwave signal generation, the proposed OEPO can also be used for computation and radio-frequency phase-stable transfer. For instance, a microwave photonic Ising machine has been proposed and demonstrated in Ref. 189 based on the binary-phase oscillation of the OEPO. This method represents a novel approach for the implementation of large-scale, high-coherence Ising machines at room temperature to accelerate the computation of ubiquitous combinatorial optimization problems.

D. Broadband OEO

In the past few decades, broadband OEOs[7,93–102] have also been constructed with an electrical bandwidth spanning at least an octave. The major difference between a broadband OEO and a traditional single-frequency OEO is that electrical filters with different bandwidths are used. Generally, lots of cavity modes are selected by a broadband filter in a broadband OEO, while only one or several modes are selected by a narrowband filter in a traditional single-frequency OEO. Fundamentally, the broadband OEO is a broadband nonlinear time-delayed system with rich and complex dynamic states, such as relaxation oscillations, chaotic breathers,

and hyperchaos, which can be used in various applications that require complex microwave waveforms. This section provides a brief introduction to the broadband OEO. We refer readers to a well-written review[7] for a detailed and comprehensive overview of this topic.

The broadband OEO is also referred to as an Ikeda-like OEO since its dynamics can be described in the form of an Ikeda-like DDE,[7,190,191]

$$\hat{\mathrm{H}}\{x(t)\} = \beta f_{\mathrm{NL}}[x(t-T)] \tag{28}$$

where $x(t)$ is a scalar dynamical variable that tracks the dynamics of the system, $\hat{\mathrm{H}}\{x(t)\}$ is a linear integrodifferential operator that is related to the loop filter of the broadband OEO, β is the linear gain, f_{NL} is a nonlinear function, and T is the time delay of the OEO cavity. In most cases, the f_{NL} of the broadband OEO is a sinusoidal function since the nonlinear function is generally provided by an interferometric device, such as a Mach–Zehnder modulator (MZM). We can see from Eq. (28) that the interplay between $\hat{\mathrm{H}}$, β, f_{NL}, and T results in rich and complex dynamical behavior of the Ikeda-like OEOs.

Based on the characteristics of the loop filter that is used in the cavity, broadband OEOs can be roughly classified as low-pass filter OEOs and broad bandpass filter OEOs. If a low-pass filter with a high-frequency cutoff f_H is used in the OEO cavity, the value of the linear integrodifferential operator $\hat{\mathrm{H}}\{x\}$ in Eq. (28) can be further determined and thus Eq. (28) can be rewritten as[7]

$$\hat{\mathrm{H}}\{x\} \equiv x + \tau\dot{x} = \beta f_{\mathrm{NL}}[x_{\mathrm{T}}], \tag{29}$$

where $\tau = 1/2\pi f_H$ is related to the high-frequency cutoff f_H of the loop filter and $x_{\mathrm{T}} \equiv x(t-T)$ is the delayed dynamical variable. For broadband OEOs with a bandpass filter, the loop filter can be considered as the joint use of a high-pass filter with cutoff frequency f_H and a low-pass filter with cutoff frequency f_L; thus, $\hat{\mathrm{H}}\{x\}$ in Eq. (28) can also be further determined and the DDE can be rewritten as[7]

$$\hat{\mathrm{H}}\{x\} \equiv \left(1+\frac{\tau}{\theta}\right)x + \tau\dot{x} + \frac{1}{\theta}\int_{t_0}^{t} x(s)ds = \beta f_{\mathrm{NL}}[x_{\mathrm{T}}], \tag{30}$$

where $\tau = 1/2\pi f_H$ and $\theta = 1/2\pi f_L$ are related to the cutoff frequencies f_H and f_L of the bandpass filter, respectively. It should be noted that generally, the high-frequency cutoff f_H is much larger than the low-frequency cutoff f_L; thus, $\left(1+\frac{\tau}{\theta}\right)x$ can be further simplified as x since $1+\frac{\tau}{\theta} \approx 1$.

The key properties of the broadband OEOs can be analyzed using the DDE, such as the evaluation of the time-domain dynamics as a function of the feedback gain β. Figure 13 shows an example of the experimental and numerical results of the time-domain dynamics of a broad bandpass filter OEO.[100] A bandpass filter with cutoff frequencies of $f_L = 3.1$ Hz and $f_H = 480$ kHz is used. The sinusoidal nonlinearity f_{NL} is provided by the MZM. Here, the scalar dynamical variable $x(t)$ denotes the electrical amplitude V(t) of the oscillating signal; the numerical simulations are carried out using the DDE. As shown in Figs. 13(b) and 13(c), as β increases beyond the oscillation threshold, the broadband OEO changes from relaxation (or slow-fast) oscillations ($\beta \approx 1.5$) to periodic breathers ($\beta \approx 2$), chaotic breathers ($\beta \approx 3$), and fully developed chaos ($\beta \approx 3.5$). Apart from its rich and complex dynamic states, the broadband OEOs have also been used in chaos communications,[192–196] chaos synchronization,[197,198] random number generation,[199,200] as well as chaotic radars and lidars.[201–205]

E. Random OEO

Typically, a closed optoelectronic feedback loop is adopted in a traditional OEO cavity. Although a high-Q factor or rich dynamic states are ensured by a closed loop, only the frequency components with multiple integers of the FSR can oscillate in the OEO cavity. As we mentioned above, this delay-controlled operation limits the potential oscillation frequency of a traditional OEO once its cavity delay is determined. As a result, the randomness of the generated broadband microwave signals of the broadband OEO and OEPO is limited. Discrete frequency components with frequencies related to the cavity delay can still be observed at the spectrum of the generated signal unless the feedback strength of the optoelectronic loop is ultra-high. One solution to overcome this problem is to use an optoelectronic parametric process in the OEO cavity, which is the method we used in the OEPO.[92] In Ref. 103, we also proposed and demonstrated a novel random OEO that overcomes the limitation of the cavity delay in a traditional OEO. Broadband random microwave signals are obtained from the random OEO cavity by using the unique features of random light scattering in an optical fiber as the feedback scheme for the oscillating signal, while maintaining an open-loop physical cavity.

The schematic diagram of the proposed random OEO is shown in Fig. 14(a).[103] The signal light generated by a laser diode is sent to a spool of dispersion compensation fiber (DCF) via an optical circulator and a wavelength division multiplexer (WDM). Due to the intrinsic random disorder in the optical fiber, Rayleigh scattering occurs in all directions while the signal light propagates along the fiber from the input z_0 to the open port z_L. The backscattered part of the signal light is recaptured by the fiber and sent to port 3 of the circulator. A Raman pump signal generated by a pump laser is also sent to the DCF to amplify the incident and backscattered signal light in the DCF and stimulate the Raman amplification process. An EDFA and an EA are also used to further boost the oscillating signal in the optoelectronic cavity. Unlike a traditional OEO that uses a physical closed loop to provide the required feedback for the oscillating signal, Rayleigh backscattering from an open DCF is used to provide the required feedback in the random OEO. At each scatter section z_i in the optical fiber, the Rayleigh scattering field $\Delta\varepsilon_b(t,z_i)$ fluctuates randomly in time. In theory, the Rayleigh scattering field $\Delta\varepsilon_b(t,z_i)$ can be described by a backscattering coefficient $\Delta\rho(z_i)$,

$$\Delta\varepsilon_b(t,z_i) = M(z_i)\varepsilon_s\left(t-\frac{2z_i}{v}\right)e^{-\alpha z_i}e^{-j2\beta z_i}\Delta\rho(z_i), \tag{31}$$

where M is the unitary Jones matrix, α is the attenuation coefficient, β is the propagation constant, v is the group velocity, and $\Delta\rho(z_i)$ is a time-independent zero-mean circular complex Gaussian random variable.[103] The total backscattered field at the input of the DCF is the superimposed field from each scatter section, which can be defined as

$$\varepsilon_b(t) = \sum_{n=1}^{N}\Delta\varepsilon_b(t,n\Delta l), \tag{32}$$

where $Nl = z_L$ is the total length of the DCF. We can see that the total backscattered field also fluctuates randomly in time. A large

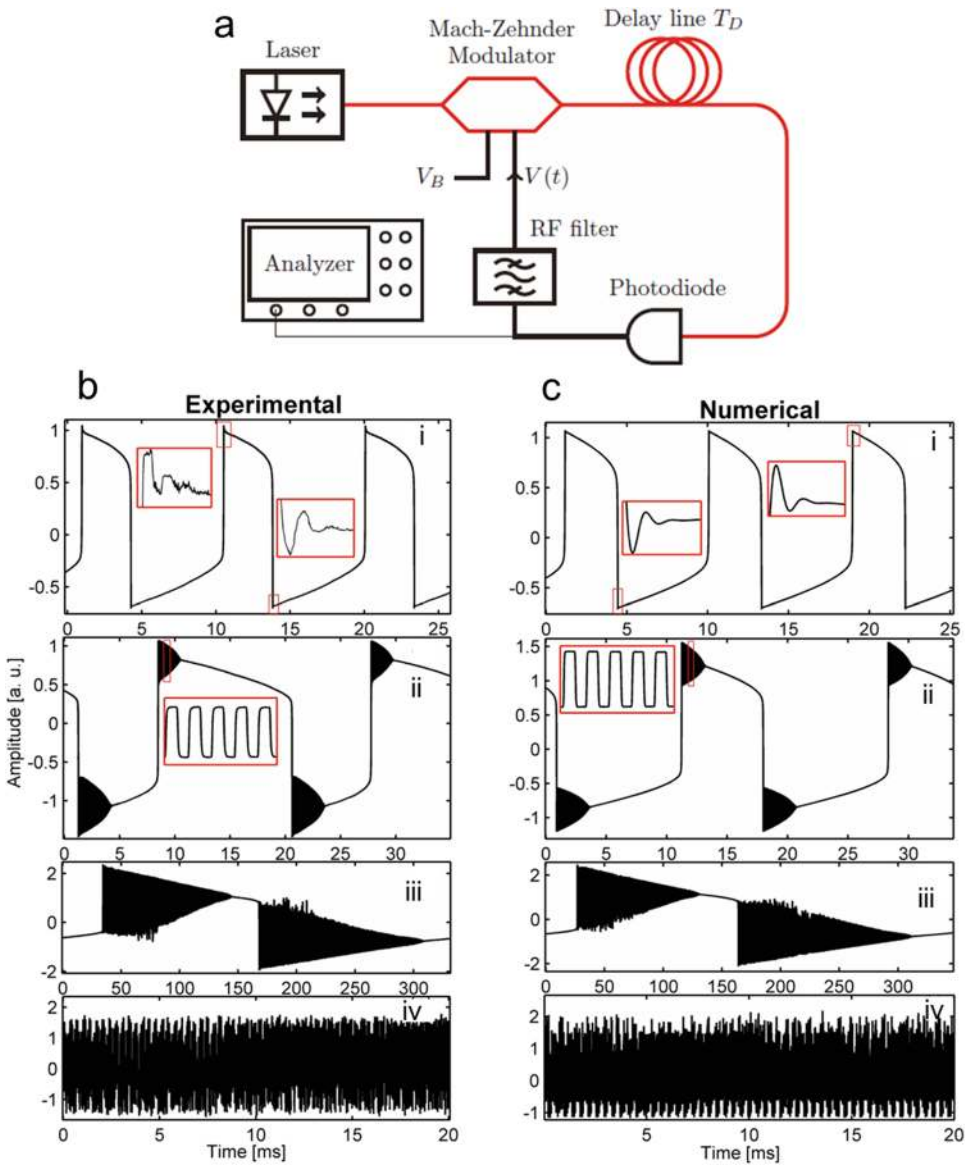

FIG. 13. A broadband OEO. (a) Schematic diagram of the OEO. A bandpass filter with cutoff frequencies of f_L = 3.1 Hz and f_H = 480 kHz is used. The sinusoidal nonlinearity f_{NL} is provided by the Mach–Zehnder modulator. (b) Experimental and (c) numerical results of the electrical amplitude V(t) for different feedback gains β. As β is increased beyond the oscillation threshold, the broadband OEO changes from (i) relaxation (or slow-fast) oscillations to (ii) periodic breathers, (iii) chaotic breathers, and (iv) fully developed chaos. Figures reproduced with permission from Mbé *et al.*, Phys. Rev. E **91**, 012902 (2015). Copyright 2015 APS.

amount of Rayleigh backscattering can be regarded as different feedback cavity lengths; thus, the random OEO can be regarded as a sum of single-loop OEOs with randomly distributed cavity lengths,

$$L_i = L_0 + 2z_i, \tag{33}$$

where L_0 is the cavity length of the OEO excluding the DCF and z_i is the scatter section at the DCF. As a result, microwave signals with different frequencies can always find the corresponding cavity lengths to oscillate in the random OEO and are not confined by the cavity delay as in the traditional OEO. Moreover, the signal power of the microwave signals also fluctuates randomly in time due to the random fluctuation of the backscattered field; thus, random microwave signals can be produced by the proposed random OEO.

Figure 14(b) shows the spectrum of the generated random microwave signal when a bandpass filter with a center frequency of 5 GHz and a bandwidth of 60 MHz is used. The inset on the left shows the frequency response of the bandpass filter, and the inset on the right shows the magnification of the spectrum. All

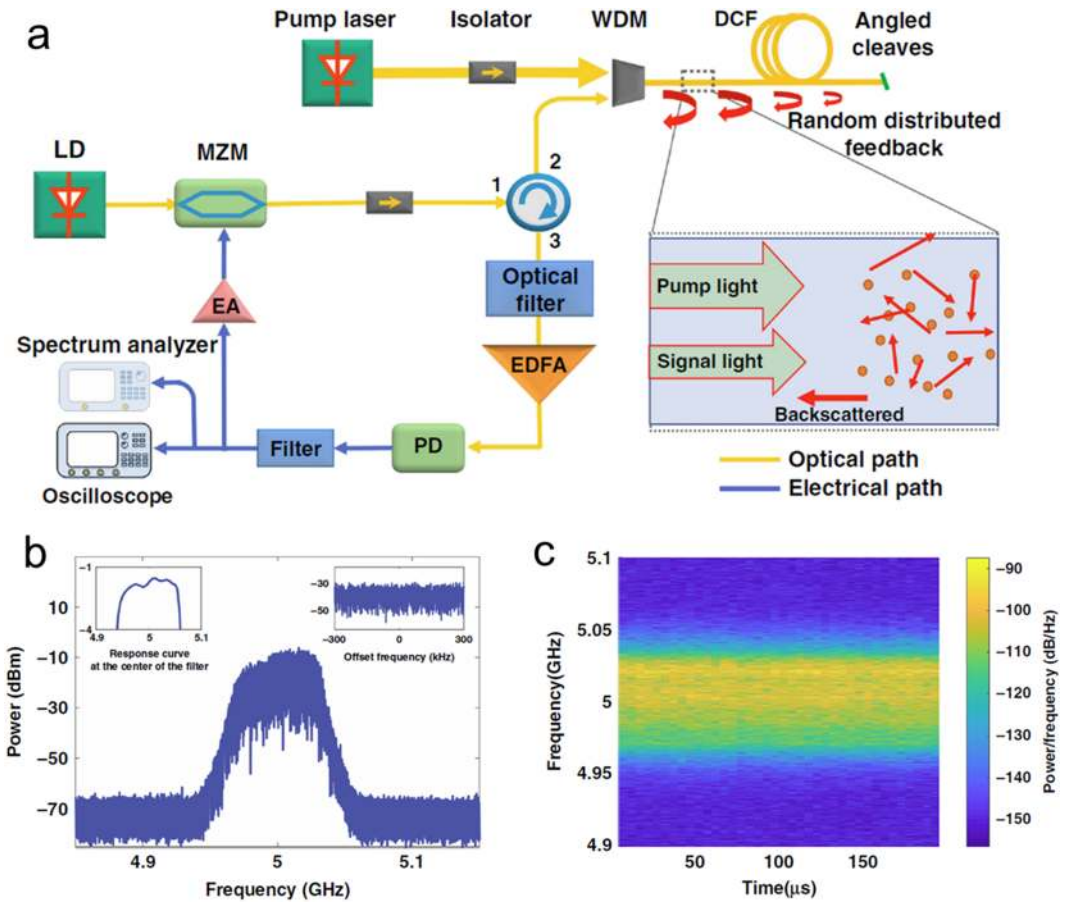

FIG. 14. A random OEO using Rayleigh light scattering in an optical fiber to provide feedback in an open-loop cavity. (a) Schematic diagram. The signal light generated by the LD is sent to the DCF via a WDM. Rayleigh scattering occurs as the signal light propagates along the optical fiber due to the intrinsic random disorder in the transmission medium. A Raman pump signal generated by the pump laser is also sent to the DCF to amplify both the incident and backscattered signal light based on the distributed Raman amplification process. The random OEO can be regarded as the sum of single-loop OEOs with randomly distributed cavity lengths, since the feedback is proved by the Rayleigh backscattering. As a result, microwave signals with different frequencies can always find the corresponding cavity lengths to oscillate in the random OEO. (b) Spectrum of the generated random microwave signal when a bandpass filter is used. The inset on the left shows the frequency response of the bandpass filter, and the inset on the right shows the magnification of the spectrum. (c) Instantaneous frequency–time diagram of the generated random microwave signal. Figures reproduced with permission from Ge *et al.*, Nat. Commun. **11**, 5724 (2020). Copyright 2020 Author(s), licensed under a Creative Commons Attribution 4.0 License.

TABLE II. Characteristics of selected mode control methods of OEOs.

Method	Type of generated signal	Characteristics	References
Tunable filtering	Tunable single-frequency microwave signal	Frequency tuning range from DC to 60 GHz	57
Fourier domain mode-locking	Chirped microwave waveform	Broad bandwidth, large time-bandwidth product up to 166 650	75
Optoelectronic parametric process	Stable phase-locked oscillation	Stable multi-mode oscillation, delay-independent frequency tuning	92
Nonlinear dynamics	Broadband complex oscillation	Rich dynamics, such as relaxation oscillation, periodic breathers, and chaos	100
Randomly distributed feedback	Random signal	Tunable wide bandwidth with frequencies up to 40 GHz	103

frequencies in the passband of the filter oscillate together without a discrete mode interval. The calculated instantaneous frequency–time diagram using a Hamming window is shown in Fig. 14(c). As can be seen, the power of the generated signal varies at different frequencies. The power of a particular frequency changes randomly in each of the two adjacent time windows. Random microwave signals with different center frequencies and bandwidths can also be produced by changing the electrical bandwidth of the random OEO. For example, ultra-wideband random microwave signals with frequencies ranging from DC to about 40 GHz have been successfully produced.[103]

Table II summarizes the approaches and characteristics of the cavity mode control of OEOs based on different methods. As can be seen, diverse microwave signals can be obtained using different mode control methods, demonstrating the significant potential of OEOs for microwave signal generation.

V. INTEGRATED OEO

Although remarkable developments have been achieved in the past few decades regarding low-phase noise microwave signal generation and cavity mode control of OEOs, the large size and high power consumption still limit the popularization of OEOs in practical applications since most of the aforementioned OEOs are implemented using discrete optical and electrical devices. With the rapid development of photonic integrated circuits (PICs), several partially integrated and even monolithically integrated OEOs[113–128] have been reported in recent years. These devices have a compact size and low power consumption.

Benefited from the rapid development of photonic integrated circuits, integration of OEOs can be achieved in different platforms, such as silicon, indium phosphide, and chalcogenide. Ideally, all the optical and electrical devices in the OEO loop should be integrated to minimize its size and high power consumption; however, a high-performance fully integrated OEO is still challenging due to the complexity or inferior performance of the integrated devices. Figure 15 shows several selected examples of integrated OEOs. A silicon-integrated OEO was proposed and demonstrated in Ref. 113, with several key optical building blocks, including a high-speed PM, a thermally tunable micro-disk resonator (MDR), and a high-speed PD. A frequency tunable MPF can be implemented based on PM-IM conversion using the above three key optical building blocks;

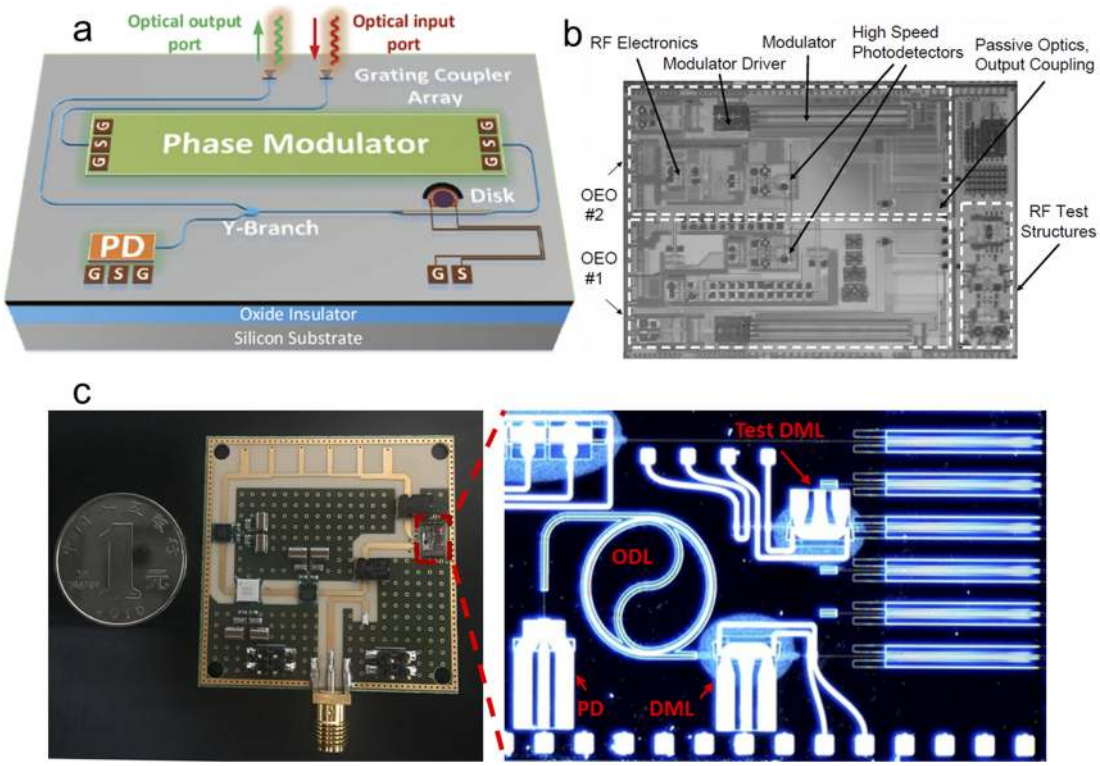

FIG. 15. Selected examples of integrated OEOs. (a) A silicon-integrated OEO with several key optical building blocks, including a high-speed PM, a thermally tunable MDR, and a high-speed PD. (b) Silicon-integrated coupled OEO. Two side-by-side OEO circuits are shown in this die micrograph. Each OEO circuit consists of an integrated optoelectronic loop and a partially integrated optical loop. Discrete optical delay and amplification devices are used to close the optical loop. (c) An integrated OEO with monolithically integrated photonic parts. All the optical devices in the OEO system are integrated on an InP chip. The electrical parts are fabricated on a printed circuit board. Panel (a) is reproduced with permission from W. Zhang and J. Yao, J. Lightwave Technol. **36**(19), 4655–4663 (2018). Copyright 2018 IEEE. Panel (b) is from Gunn, *Proceedings of the 54th IEEE International Solid-State Circuits Conference (ISSCC '07)*. Copyright 2007 IEEE. Reproduced with permission from IEEE. Panel (c) is reproduced with permission from Hao *et al.*, J. Lightwave Technol. **36**(19), 4565–4582 (2018). Copyright 2018 IEEE.

TABLE III. Comparison of selected integrated OEOs.

Platform	Level of integration	Phase noise	References
Silicon	Partially integrated photonic parts	−80 dBc/Hz @ 10 KHz for 6.8-GHz signal	113
Silicon	Partially integrated photonic parts and monolithically integrated electrical parts	−112dBc/Hz @10 kHz for 10.2-GHz signal (with external ODE)	114
Indium phosphide	Monolithically integrated photonic parts	−92 dBc/Hz @1 MHz for 8.87-GHz signal	115
Chalcogenide	Partially integrated photonic parts	About −90 dBc/Hz@10 kHz for 10.9-GHz signal	126

thus, the silicon-integrated OEO also has good frequency tunability. The measured phase noise of the generated microwave signal is about −80 dBc/Hz at 10 KHz offset. One significant advantage of silicon photonics is the seamless integration of optical and electrical devices due to the compatibility with mature electrical CMOS technology. A silicon-integrated COEO with hybrid integration of photonic and electronic parts was reported in Ref. 114 and its die micrograph is shown in Fig. 15(b). All the electrical devices and a silicon Mach–Zehnder Interferometer (MZI) modulator are integrated. The optical loop is closed using a semiconductor optical amplifier (SOA) and an optical delay element (ODE) placed outside the integrated chip. By using a long external ODE, a low phase noise of −112dBc/Hz at a 10 kHz offset has been achieved. Nevertheless, the integration of active optical devices, such as lasers and optical amplifiers, represents a challenge for silicon photonics.[206,207] Active optical devices can be integrated on a chip using an InP platform. An integrated OEO with monolithically integrated photonic parts was reported in Ref. 115. All the optical devices in the OEO system are integrated on the InP chip, and the electrical parts are fabricated on a printed circuit board (PCB). A comparison of selected integrated OEOs is listed in Table III. As can be seen, the phase noise of the integrated OEOs without an external ODE is still poor due to the fact that its total loop delay T in Eq. (13) is very small. The total loop delay can be further enhanced to ensure a lower phase noise, for example by using a low-loss silicon nitride waveguide.

VI. OTHER APPLICATIONS OF OEO

In addition to the distinct features of microwave and optical signal generation, emerging applications of OEO in sensing, computing, signal processing, and other research fields have also been intensively investigated and attracted much attention. Some of the important applications of OEO reported in recent years are reviewed in this section.

A. Sensing

OEO-based sensors can be implemented by mapping the measurand-dependent parameter change to the frequency change of the generated microwave signal of the OEO.[129–141] Due to the high resolution and high speed of the frequency measurements in the electrical domain, OEO-based sensors have high resolution and high speed, which are both much higher than traditional optical sensor systems using an optical spectrum analyzer. In addition, the microwave signal generated by the OEO has a high signal-to-noise ratio (SNR), ensuring a high SNR of the OEO-based sensor. In recent years, various approaches have been proposed and demonstrated to measure target parameters, such as the strain, refractive index, transverse load, distance, temperature, and acoustic characteristics of OEOs.[129–141]

An example of an OEO-based strain sensor[132] is shown in Fig. 16. The fundamental concept is to convert the strain-induced wavelength change to the frequency change of a generated microwave signal of the dual-loop OEO. A MPF based on PM-IM conversion is adopted in the OEO cavity. A dual-loop OEO using a PM-IM conversion-based MPF is adopted. Similar to the MPF in Fig. 11, a PS-FBG is also used in this scheme as an optical notch filter to change the balance of phase modulation. The center frequency of the MPF is determined by the frequency difference between the laser diode and the PS-FBG. When a strain is applied to the PS-FBG, the frequency of the notch of the PS-FBG would be changed. As a result, the center frequency of the MPF and the oscillation frequency of the OEO change as the applied strain of the PS-FBG is changed; thus, strain sensing can be achieved by measuring the frequency of the generated microwave signal. The measured frequency responses of the MPF and the spectra of OEO for different strain levels are shown in Figs. 16(b) and 16(c), respectively. As can be seen, the SNR of the generated microwave signal is about 70 dB, which is very large compared with other techniques. A linear relationship between the oscillation frequency of the OEO and the applied strain is observed in Fig. 16(d), which is also consistent with the theory.

B. Computing

Computing is another important application of OEOs. As a time-delayed optoelectronic system, broadband OEOs have been proposed and demonstrated as a hardware platform for reservoir computing.[7,142] A wide variety of tasks, such as pattern recognition and time-series prediction, have been successfully implemented using OEO-based reservoir computers.[143–149]

An Ising machine based on an OEO was proposed for solving optimization problems.[150] The Ising machine is an analog system that maps optimization problems to Ising models, solving the optimization problems by finding the ground state of the Ising machine. Compared with conventional algorithms, an Ising machine operates considerably faster since it can evolve to the ground state rapidly. Ising machines based on various analog systems have been demonstrated previously, such as quantum annealers based on superconducting circuits and coherent Ising machines based on optical parametric oscillators (OPOs). Although solving optimization problems has been achieved successfully, the operation of the quantum annealers must be under an ultra-low temperature of millikelvin and the OPO-based Ising machines are sensitive to environmental changes. The two problems can be solved by implementing the Ising machine

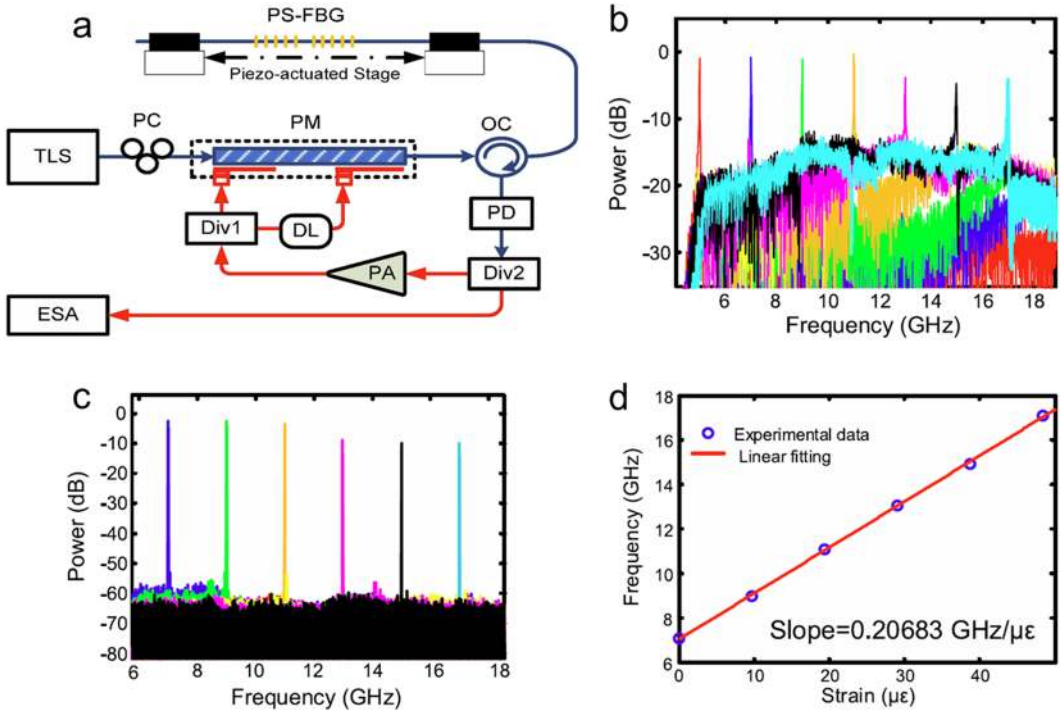

FIG. 16. A strain sensor based on an OEO. (a) Block diagram. A dual-loop frequency tunable OEO based on PM-IM conversion using a PS-FBG is adopted. The center frequency of the MPF and the oscillation frequency of the OEO change as the applied strain of the PS-FBG is changed; thus, strain sensing can be achieved by measuring the frequency of the generated microwave signal. (b) Measured frequency responses of the MPF as the applied strain is changed. (c) Measured spectra of OEO as the applied strain is changed. (d) Relationship between the oscillation frequency and applied strain. LD, laser diode; PC, polarization controller; PM, phase modulator; OC, optical circulator; PS-FBG, phase-shifted fiber Bragg grating; PD, photodetector; EC, electrical coupler; EA, electrical amplifier; DL, delay line; and ESA, electrical spectrum analyzer. Figures from Li *et al.*, *Proceedings of IEEE Photonics Conference*. Copyright 2012 IEEE. Reproduced with permission from IEEE.

based on an OEO. The energy function of the Ising Machine is represented by the Ising Hamiltonian $H_{Ising} = -\frac{1}{2}\sum_{mn}^{N} J_{mn}\sigma_m\sigma_n$, where N is the number of the coupled spins, J_{mn} is the spin interaction matrix, and σ_m and σ_n are the z projection of the spins with binary eigenvalues of 1 or −1. The optimization problems are mapped to the Ising Machines by spin coupling using the spin interaction matrix J_{mn}, and the solution of the optimization problems is related to the ground state of the Ising machine. In the OEO-based Ising machine, the artificial spins are represented by the photovoltage generated in the OEO cavity. Due to the feedback-induced bifurcation of the OEO, a pitchfork bifurcation occurs near the oscillation threshold. The OEO has two stable fixed points above the bifurcation point; thus, Ising spin networks can be implemented by mapping the photovoltage to the Ising spin. The schematic diagram and working principle of the iteration process are shown in Fig. 17. As can be seen, an N-spin network is achieved by dividing the photovoltage into N equal intervals in the time domain. Spin coupling is achieved in the digital hardware by performing matrix multiplication. Up to 100 spins were executed in an experiment, achieving excellent performance for solving MAXCUT optimization problems.[150]

C. Signal processing

The use of OEOs in electrical and optical signal processing has also been proposed and demonstrated. For example, photonic microwave upconversion and downconversion[152–154] have been implemented using the OEOs as local oscillators. This application has attracted significant attention for radio-over-fiber systems. Clock recovery has also been reported due to injection locking in OEOs.[155–165] In this system, the OEO is injection locked to the clock of an incoming electrical or optical stream of data. The OEO output is thereby synchronized with the incoming data stream. Due to the wide bandwidth of OEOs, high-frequency data streams can be successfully recovered. Multichannel optical signal processing has also been achieved in these OEOs in addition to clock recovery, such as modulation format conversion.[164] Moreover, clock division,[166] microwave frequency division,[167–169] signal channelization, and low-power RF signal detection[170–175] using OEOs have also been demonstrated based on the injection locking process. Figure 18 shows an example of a low-power RF signal detection scheme based on a multimode OEO.[171] The detection of low-power RF signals is crucial in applications such as modern radar, electronic warfare, and radio astronomy, since the RF signals are generally low in the cluttered environment. Although low-power RF signal detection can be implemented in the electrical domain, the frequency range and instantaneous bandwidth are limited due to the electronic bottleneck. On the other hand, low-power RF signal detection based on an OEO offer promising advantages, such as wide frequency range and large bandwidth. The cavity mode in the multimode OEO can only

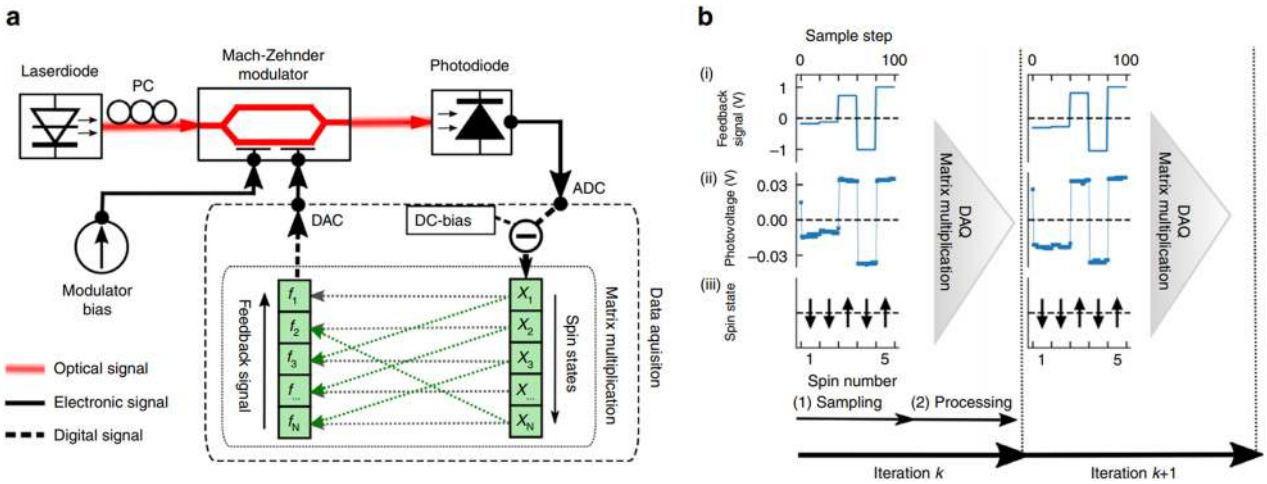

FIG. 17. An OEO-based Ising machine for solving optimization problems. (a) Schematic diagram. The artificial spins in the OEO-based Ising machine are generated in a feedback-induced bifurcation process and are represented by the photovoltage. An N-spin network is achieved by dividing the photovoltage into N equal intervals in the time domain. Spin coupling is achieved in the digital hardware by performing matrix multiplication. (b) Working principle of spin coupling during two consecutive iterations. Each iterations includes a sampling stage and a processing stage to update the photovoltage and feedback signal. Figures reproduced from Böhm *et al.*, Nat. Commun. **10**, 3538 (2019). Copyright 2019 Author(s), licensed under a Creative Commons Attribution 4.0 License.

oscillate if an RF signal with an appropriate frequency is injected since the gain of the multimode OEO is just below the oscillation threshold. The measured spectrum when a 1.0022-GHz RF signal with a power of −70 dBm is injected into the OEO cavity is shown in the right part of Fig. 18. It is observed that low-power RF signals can be selectively amplified if their frequency is matched with that of the cavity modes of OEO.

Microwave frequency measurement is another OEO application in signal processing. Traditional electrical microwave frequency measurement methods can achieve a high resolution, but the measurement range is generally limited to several of GHz and the system is sensitive to electromagnetic interference (EMI). Using the OEO-based scheme, the measurement range can be easily extended to tens of GHz, and the system is immune to EMI. Recently, we reported a microwave frequency measurement scheme based on the FDML OEO.[90] The principle and measured results are shown in Fig. 19. The key to the proposed scheme is frequency-to-time mapping in the FDML OEO cavity, and the unknown microwave frequency is measured using the time-domain information.

As we reported in Sec. IV, frequency scanning microwave signals with instantaneous frequencies that change over time can be generated by the FDML OEO. In the proposed microwave

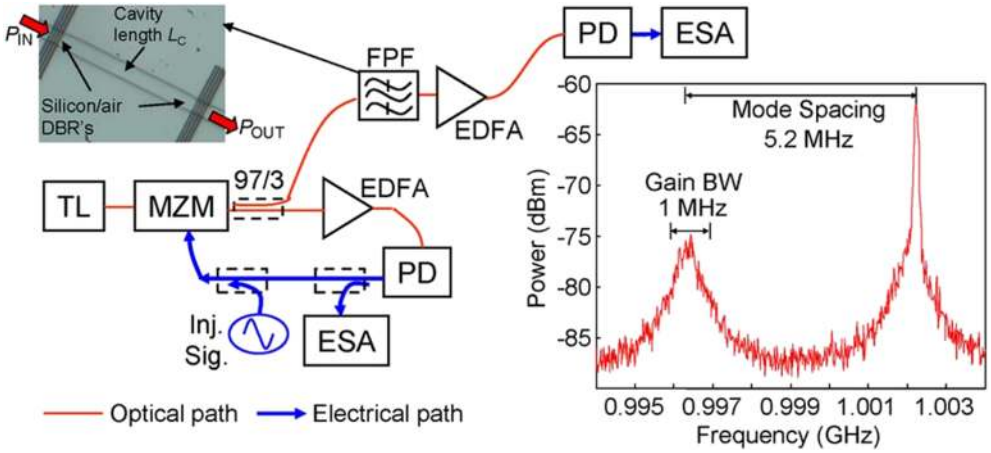

FIG. 18. Selective amplification and detection of low-power RF signals based on an OEO. Left: experimental setup. The gain of the OEO is maintained just below the threshold. The low-power RF signal is injected into the multimode OEO and is selectively amplified if its frequency is matched with that of the cavity modes of the OEO. Right: measured spectrum when a 1.0022-GHz RF signal with a power of −70 dBm is injected into the OEO cavity. A gain of 8-dB is achieved. Figures reproduced with permission from Devgan *et al.*, IEEE Photonics Technol. Lett. **22**(3), 152–154 (2010). Copyright 2010 IEEE.

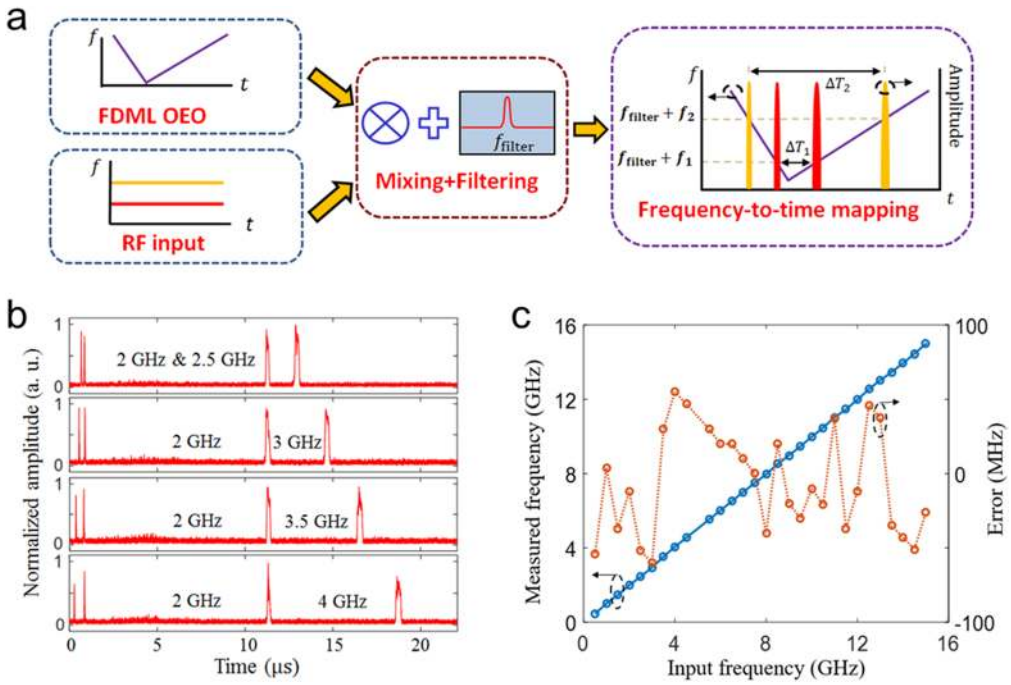

FIG. 19. Microwave frequency measurement based on a FDML OEO. (a) Principle of the microwave frequency measurement system. The unknown microwave signal can be measured in the time domain based on frequency-to-time-mapping that established in the FDML OEO cavity. The microwave signal under test is injected into the FDML OEO cavity and is mixed with the chirped microwave signal of the FDML OEO at the photodetector. By filtering the beat-note signal using a single-passband filter, frequency-to-time mapping can be achieved and thus can be used for frequency measurements. (b) Amplitude of the time domain waveform when a two-tone microwave signal is injected into the FDML OEO. (c) Measured frequency and corresponding errors. Figures reproduced with permission from Hao *et al.*, Opt. Express **26**(26), 33582–33591 (2018). Copyright 2018 OSA.

TABLE IV. Selected OEO applications in sensing, computing, and signal processing. WER, word error rate; NMSE, normalized mean square error; NRZ, nonreturn-to-zero; RZ, return-to zero; and (CSRZ) carrier-suppressed return-to-zero.

Application	Function	Characteristics	References
Sensing	Refractive index sensing	Uncertainty: 10^{-2}; slope −226.62 ±2.53 kHz/mm	131
	Strain sensing	Resolution: 360 fm; SNR: 70 dB; slope 0.206 683 GHz/με	132
	Transverse load sensing	Sensitivity: 9.73 GHz/(N/mm); minimal detectable load: 2.06×10^{-4} N/mm	133
	Acoustic sensing	Spectral resolution: Sub-Hertz	134
	Distance measurement	Resolution: 1.5 μm/Hz; standard deviation: 14.8 μm	135
	Temperature sensing	Sensitivity: 3.7 MHz/°C; repeatability error: Less than 0.02%	140
Computing	Reservoir computing	Nodes: 400; spoken digit recognition with WER of 0.04%; time series prediction with NMSE of 12%	143
	Ising machine	Spin number: 100; success rate: 90% for a square lattice and 34% for a Möbius ladder graph	150
Signal processing	Frequency conversion	Frequency upconversion to the 20-GHz band	152
	Clock recovery	Clock frequency: 100 MHz and 4.95 GHz, can be extended to 70 GHz in theory	155
	Modulation format conversion	NRZ-to-RZ/CSRZ conversion	164
	Microwave frequency division	Division ratio: 2 and 3; frequency range: 4.51–34.88 GHz	169
	Signal channelization and low-power RF signal detection	Sensitivity: −83 dBm; compression dynamic range: 72 dB; frequency range: 1–6 GHz	171
	Frequency measurement	Resolution: 60 MHz; frequency range: 1–15 GHz	90

frequency measurement scheme, the bi-directional frequency scanning microwave signal generated by the FDML OEO is mixed with the microwave signal under test by injecting the microwave signal into the FDML OEO cavity. A single-passband filter is also used to select a portion of the mixed product. In the time domain, the output of the filter is periodical pulse trains due to the bi-directional frequency scanning property of the FDML OEO. For example, an output pulse can only be observed at the output of the single-passband filter when the frequency component $f_{\text{filter}} + f_1$ of the frequency scanning microwave signal is mixed with the microwave signal under test if the frequency of microwave signal under test is f_1. There are two output pulses within one scanning period, thanks to the bi-directional frequency scanning property of FDML OEO. The time difference between the output pulses within one scanning period of the FDML OEO is related to the frequency of the injected microwave signal; thus, frequency-to-time mapping is established and used for microwave frequency measurements. Single and multiple-tone microwave signals can also be measured by the proposed system, which is difficult to achieve for many photonic-assisted frequency measurement systems.[208–210] Figure 19(b) shows the amplitude of the time-domain waveform when a two-tone microwave signal is injected. As expected, two pairs of output pulses are observed in the time domain. The measured frequency and corresponding errors are shown in Fig. 19(b). The measurement errors are less than 60 MHz. In addition, the single-passband filter can also be removed from the frequency measurement system by using a FDML OEO operating around threshold.[91] OEO applications in sensing, computing, and signal processing are summarized in Table IV.

VII. CONCLUSIONS

We reviewed the basic operating principle and the key phase noise performance of OEOs. Several approaches for generating spectrally pure low phase noise microwave signals have been summarized, such as dual-loop OEO, OEO based on a high-Q ring resonator, COEO, and PT-symmetric OEO. In addition to its phase noise performance, the long-term frequency stability should be considered in practical applications. Long-term frequency stabilization methods, such as injection locking and phase locking, were discussed. Oscillation mode control techniques were described, such as tunable signal frequency signal generation using tunable filters, chirped signal generation using Fourier domain mode-locking, stable multi-mode oscillation based on a nonlinear parametric process, complex oscillation based on nonlinear dynamics, and random oscillation based on random scattering. Versatile microwave signals can be obtained using OEOs using these mode control techniques. Examples of integrated OEOs with a compact size and low power consumption were also provided. In addition to signal generation, OEOs have also been used in other applications. Selected application scenarios were discussed, such as sensing, computing, and signal processing.

In summary, OEOs have been widely investigated in various research fields due to their attractive features, including ultra-low phase noise, frequency flexibility, and versatility in diverse applications. Fiber-based OEOs have an excellent phase noise performance, but they also have a large size and high power consumption. Compact size and low power consumption have been achieved using integrated OEOs; however, these OEOs have increased phase noise. Novel schemes or high Q-factor schemes should be developed to ensure low phase noise in integrated OEOs. In addition to single-frequency microwave signals, several complex microwave waveforms have been generated using OEOs. The generation of new kinds of microwave waveforms is expected due to the intrinsic multimode cavity of OEOs. Moreover, the applications of OEOs might be further extended in the near future owing to the unique properties of the hybrid optoelectronic feedback system.

ACKNOWLEDGMENTS

This work was supported by the National Key Research and Development Program of China (Grant Nos. 2018YFB2201902, 2018YFB2201901, and 2018YFB2201903) and the National Natural Science Foundation of China (Grant Nos. 61925505, 61535012, and 61705217).

DATA AVAILABILITY

The data that support the findings of this study are available from the corresponding author upon reasonable request.

REFERENCES

[1] X. S. Yao and L. Maleki, "High frequency optical subcarrier generator," Electron. Lett. **30**(18), 1525–1526 (1994).
[2] X. S. Yao and L. Maleki, "Optoelectronic oscillator for photonic systems," IEEE J. Quantum Electron. **32**(7), 1141–1149 (1996).
[3] X. S. Yao and L. Maleki, "Optoelectronic microwave oscillator," J. Opt. Soc. Am. B **13**(8), 1725–1735 (1996).
[4] X. S. Yao and L. Maleki, "Converting light into spectrally pure microwave oscillation," Opt. Lett. **21**, 483–485 (1996).
[5] L. Maleki, "The optoelectronic oscillator," Nat. Photonics **5**, 728–730 (2011).
[6] L. Maleki, "The opto-electronic oscillator (OEO): Review and recent progress," in *European Frequency and Time Forum* (IEEE, Gothenburg, Sweden, 2012), pp. 497–500.
[7] Y. K. Chembo, D. Brunner, M. Jacquot, and L. Larger, "Optoelectronic oscillators with time-delayed feedback," Rev. Mod. Phys. **91**, 035006 (2019).
[8] T. Hao *et al.*, "Recent advances in optoelectronic oscillators," Adv. Photonics **2**(4), 044001 (2020).
[9] G. R. Huggett, "Modelocking of CW lasers by regenerative RF feedback," Appl. Phys. Lett. **13**, 186–187 (1968).
[10] R. T. Kersten, "Ein optisches nachrichtensystem mit bauelementen der integrierten optik für die übertragung hoher bitraten," Arch. Elektrotech. **60**(6), 353–359 (1978).
[11] D. Eliyahu, D. Seidel, and L. Maleki, "Phase noise of a high performance OEO and an ultra low noise floor cross-correlation microwave photonic homodyne system," in *IEEE International Frequency Control Symposium* (IEEE, Honolulu, HI, 2008), pp. 19–21.
[12] X. S. Yao, L. Maleki, Y. Ji, G. Lutes, and M. Tu, "Dual-loop optoelectronic oscillator," in *Proceedings of the IEEE International Frequency Control Symposium(FCS '98)* (IEEE, 1998), pp. 545–549.
[13] J. Yang, Y. Jin-Long, W. Yao-Tian, Z. Li-Tai, and Y. En-Ze, "An optical domain combined dual-loop optoelectronic oscillator," IEEE Photonics Technol. Lett. **19**(11), 807–812 (2007).
[14] S. Jia *et al.*, "A novel optoelectronic oscillator based on wavelength multiplexing," IEEE Photonics Technol. Lett. **27**(2), 213–216 (2014).
[15] X. S. Yao and L. Maleki, "Multiloop optoelectronic oscillator," IEEE J. Quantum Electron. **36**(1), 79–84 (2000).
[16] T. Bánky, B. Horváth, and T. Berceli, "Optimum configuration of multiloop optoelectronic oscillators," J. Opt. Soc. Am. B **23**(7), 1371–1380 (2006).

[17]T. Berceli, T. Bánky, and B. Horváth, "Opto-electronic generation of stable and low noise microwave signals," IEE Proc.: Optoelectron. **153**(3), 119–127 (2006).
[18]E. Shumakher and G. Eisenstein, "A novel multiloop optoelectronic oscillator," IEEE Photonics Technol. Lett. **22**(20), 1881–1883 (2008).
[19]X. S. Yao and L. Maleki, "Dual microwave and optical oscillator," Opt. Lett. **22**(24), 1867–1869 (1997).
[20]X. S. Yao, L. Davis, and L. Maleki, "Coupled optoelectronic oscillators for generating both RF signal and optical pulses," J. Lightwave Technol. **18**(1), 73–78 (2000).
[21]X. S. Yao, L. Maleki, and V. Ilchenko, "Opto-electronic oscillators having optical resonators," U.S. patent 6567436 (20 May 2003).
[22]X. S. Yao, L. Maleki, and V. Ilchenko, "Integrated opto-electronic oscillator having optical resonators," U.S. patent 6873631 (29 March 2005).
[23]J. Lasri, P. Devgan, R. Tang, and P. Kumar, "Self-starting optoelectronic oscillator for generating ultra-low-jitter high-rate (100 GHz or higher) optical pulses," Opt. Express **11**(12), 1430–1435 (2003).
[24]D. Dahan, E. Shumakher, and G. Eisenstein, "Self-starting ultralow-jitter pulse source based on coupled optoelectronic oscillators with all intracavity fiber parametric amplifier," Opt. Lett. **30**(13), 1623–1625 (2005).
[25]C. Williams, J. Davila-Rodriguez, D. Mandridis, and P. J. Delfyett, "Noise characterization of an injection-locked COEO with long-term stabilization," J. Lightwave Technol. **29**(19), 2906–2912 (2011).
[26]W. Zhou and G. Blasche, "Injection-locked dual opto-electronic oscillator with ultra-low phase noise and ultra-low spurious level," IEEE Trans. Microwave Theory Tech. **53**(3), 929–933 (2005).
[27]O. Okusaga, E. J. Adles, E. C. Levy, W. Zhou, G. M. Carter, C. R. Menyuk, and M. Horowitz, "Spurious mode reduction in dual injection-locked optoelectronic oscillators," Opt. Express **19**(7), 5839–5854 (2011).
[28]K.-H. Lee, J.-Y. Kim, and W.-Y. Choi, "Injection-locked hybrid optoelectronic oscillators for single-mode oscillation," IEEE Photonics Technol. Lett. **20**, 1645–1647 (2008).
[29]O. Okusaga, W. Zhou, E. C. Levy, M. Horowitz, G. M. Carter, and C. R. Menyuk, "Experimental and simulation study of dual injection-locked OEOs," in *IEEE International Frequency Control Symposium* (IEEE, 2009), pp. 875–879.
[30]Y. Liu, T. Hao, W. Li, J. Capmany, N. Zhu, and M. Li, "Observation of parity-time symmetry in microwave photonics," Light: Sci. Appl. **7**(1), 38 (2018).
[31]J. Zhang and J. Yao, "Parity-time symmetric optoelectronic oscillator," Sci. Adv. **4**(6), eaar6782 (2018).
[32]L. Li, G. Wang, J. Zhang, and J. Yao, "A parity-time-symmetric optoelectronic oscillator based on dual-wavelength carriers in a single spatial optoelectronic loop," in *International Topical Meeting on Microwave Photonics (MWP)* (IEEE, Ottawa, ON, 2019), pp. 1–4.
[33]J. Zhang *et al.*, "Parity-time symmetry in wavelength space within a single spatial resonator," Nat. Commun. **11**, 3217 (2020).
[34]Z. Fan, W. Zhang, Q. Qiu, and J. Yao, "Hybrid frequency-tunable parity-time-symmetric optoelectronic oscillator," J. Lightwave Technol. **38**, 2127–2133 (2020).
[35]Z. Dai, Z. Fan, P. Li, and J. Yao, "Frequency-tunable parity-time-symmetric optoelectronic oscillator using a polarization-dependent sagnac loop," J. Lightwave Technol. **38**(19), 5327–5332 (2020).
[36]C. Teng *et al.*, "Fine tunable PT-symmetric optoelectronic oscillator based on laser wavelength tuning," IEEE Photonics Technol. Lett. **32**(1), 47–50 (2020).
[37]P. Li, Z. Dai, Z. Fan, L. Yan, and J. Yao, "Parity–time-symmetric frequency-tunable optoelectronic oscillator with a single dual-polarization optical loop," Opt. Lett. **45**, 3139–3142 (2020).
[38]F. Zou *et al.*, "Parity-time symmetric optoelectronic oscillator based on an integrated mode-locked laser," IEEE J. Quantum Electron. **57**(2), 5000209 (2021).
[39]Q. Ding, M. Wang, J. Zhang, H. Mu, C. Wang, and G. Fan, "A precisely frequency-tunable parity-time-symmetric optoelectronic oscillator," J. Lightwave Technol. **38**, 6569–6577 (2020).
[40]C. Teng, X. Zou, P. Li, W. Pan, and L. Yan, "Wideband frequency-tunable parity-time symmetric optoelectronic oscillator based on hybrid phase and intensity modulations," J. Lightwave Technol. **38**(19), 5406–5411 (2020).
[41]J. Fan, L. Li, J. Zhang, X. Feng, B. Guan, and J. Yao, "A parity-time-symmetric optoelectronic oscillator based on non-reciprocal electro-optic modulation," J. Lightwave Technol. **39**(8), 2305–2310 (2021).
[42]A. Matsko, L. Maleki, A. Savchenkov, and V. Ilchenko, "Whispering gallery mode based optoelectronic microwave oscillator," J. Mod. Opt. **50**(17), 2523–2542 (2003).
[43]K. Volyanskiy, P. Salzenstein, H. Tavernier, M. Pogurmirskiy, Y. K. Chembo, and L. Larger, "Compact optoelectronic microwave oscillators using ultra-high Q whispering gallery mode disk-resonators and phase modulation," Opt. Express **18**(21), 22358–22363 (2010).
[44]K. Saleh and Y. K. Chembo, "Phase noise performance comparison between microwaves generated with Kerr optical frequency combs and optoelectronic oscillators," Electron. Lett. **53**, 264–266 (2017).
[45]D. Eliyahu, W. Liang, E. Dale, A. A. Savchenkov, V. S. Ilchenko, A. B. Matsko, D. Seidel, and L. Maleki, "Resonant widely tunable opto-electronic oscillator," IEEE Photonics Technol. Lett. **25**, 1535–1538 (2013).
[46]D. Eliyahu and L. Maleki, "Tunable, ultra-low phase noise YIG based opto-electronic oscillator," in *IEEE MTT-S International Microwave Symposium Digest, 2003* (IEEE, 2003), pp. 2185–2187.
[47]E. Shumakher, S. Ó Dúill, and G. Eisenstein, "Optoelectronic oscillator tunable by an SOA based slow light element," J. Lightwave Technol. **27**(18), 4063–4068 (2009).
[48]S. Pan and J. Yao, "Wideband and frequency-tunable microwave generation using an optoelectronic oscillator incorporating a Fabry–Perot laser diode with external optical injection," Opt. Lett. **35**(11), 1911–1913 (2010).
[49]W. Li and J. Yao, "An optically tunable optoelectronic oscillator," J. Lightwave Technol. **28**(18), 2640–2645 (2010).
[50]M. Li, W. Li, and J. Yao, "Tunable optoelectronic oscillator incorporating a high-Q spectrum-sliced photonic microwave transversal filter," IEEE Photonics Technol. Lett. **24**(14), 1251–1253 (2012).
[51]Z. Tang, S. Pan, D. Zhu, R. Guo, Y. Zhao, M. Pan, D. Ben, and J. Yao, "Tunable optoelectronic oscillator based on a polarization modulator and a chirped FBG," IEEE Photonics Technol. Lett. **24**(17), 1487–1489 (2012).
[52]D. Zhu, S. Pan, and D. Ben, "Tunable frequency-quadrupling dual-loop optoelectronic oscillator," IEEE Photonics Technol. Lett. **24**(3), 194–196 (2012).
[53]W. Li and J. Yao, "Wideband frequency-tunable optoelectronic oscillator incorporating a tunable microwave-photonic filter based on phase-modulation to intensity modulation conversion using a phase-shifted fiber-Bragg grating," IEEE Trans. Microwave Theory Tech. **60**(6), 1735–1742 (2012).
[54]B. Yang, X. Jin, X. Zhang, S. Zheng, H. Chi, and Y. Wang, "A wideband frequency-tunable optoelectronic oscillator based on a narrowband phase-shifted FBG and wavelength tuning of laser," IEEE Photonics Technol. Lett. **24**(1), 73–75 (2012).
[55]F. Jiang *et al.*, "An optically tunable wideband optoelectronic oscillator based on a bandpass microwave photonic filter," Opt. Express **21**(14), 16381–16389 (2013).
[56]X. Xie *et al.*, "Wideband tunable optoelectronic oscillator based on a phase modulator and a tunable optical filter," Opt. Lett. **38**(5), 655–657 (2013).
[57]H. Peng *et al.*, "Tunable DC-60 GHz RF generation utilizing a dual-loop optoelectronic oscillator based on stimulated Brillouin scattering," J. Lightwave Technol. **33**(13), 2707–2715 (2015).
[58]H. Peng *et al.*, "Wideband tunable optoelectronic oscillator based on the deamplification of stimulated Brillouin scattering," Opt. Express **25**(9), 10287–10305 (2017).
[59]H. Tang, Y. Yu, Z. Wang, L. Xu, and X. Zhang, "Wideband tunable opto-electronic oscillator based on a microwave photonic filter with an ultranarrow passband," Opt. Lett. **43**(10), 2328–2331 (2018).
[60]M. Shi, L. Yi, W. Wei, and W. Hu, "Generation and phase noise analysis of a wide optoelectronic oscillator with ultra-high resolution based on stimulated Brillouin scattering," Opt. Express **26**(13), 16113–16124 (2018).
[61]Z. Zeng *et al.*, "Stable and finely tunable optoelectronic oscillator based on stimulated Brillouin scattering and an electro-optic frequency shift," Appl. Opt. **59**(3), 589–594 (2020).
[62]T. Sakamoto, T. Kawanishi, and M. Izutsu, "Optoelectronic oscillator using push-pull Mach–Zehnder modulator biased at null point for optical two-tone signal generation," in *Proceedings of the Conference on Lasers and Electro-Optics* (IEEE, Baltimore, MD, 2005), pp. 877–879.

[63]M. Shin, V. S. Grigoryan, and P. Kumar, "Frequency-doubling optoelectronic oscillator for generating high-frequency microwave signals with low phase noise," Electron. Lett. **43**(4), 242–244 (2007).
[64]S. Pan and J. Yao, "A frequency-doubling optoelectronic oscillator using a polarization modulator," IEEE Photonics Technol. Lett. **21**(13), 929–931 (2009).
[65]L. Wang, N. Zhu, W. Li, and J. Liu, "A frequency-doubling optoelectronic oscillator based on a dual-parallel Mach–Zehnder modulator and a chirped fiber Bragg grating," IEEE Photonics Technol. Lett. **23**(22), 1688–1690 (2011).
[66]C. Li *et al.*, "Frequency-multiplying optoelectronic oscillator with a tunable frequency multiplication technique," Opt. Eng. **55**(12), 126110 (2016).
[67]W. Li and J. Yao, "An optically tunable frequency-multiplying optoelectronic oscillator," IEEE Photonics Technol. Lett. **24**(10), 812–814 (2012).
[68]X. Liu, W. Pan, X. Zou, D. Zheng, L. Yan, and B. Luo, "Frequency-doubling optoelectronic oscillator using DSB-SC modulation and carrier recovery based on stimulated Brillouin scattering," IEEE Photonics J. **5**(2), 6600606 (2013).
[69]W. Li, J. G. Liu, and N. H. Zhu, "A widely and continuously tunable frequency doubling optoelectronic oscillator," IEEE Photonics Technol. Lett. **27**(13), 1461–1464 (2015).
[70]C. Li *et al.*, "Frequency-sextupling optoelectronic oscillator using a Mach–Zehnder interferometer and a FBG," IEEE Photonics Technol. Lett. **28**(12), 1356–1359 (2016).
[71]L. Huang *et al.*, "Generation of triangular pulses based on an optoelectronic oscillator," IEEE Photonics Technol. Lett. **27**(23), 2500–2503 (2015).
[72]W. Y. Wang, W. Li, W. H. Sun, W. Wang, J. G. Liu, and N. H. Zhu, "Triangular microwave waveforms generation based on an optoelectronic oscillator," IEEE Photonics Technol. Lett. **27**(5), 522–525 (2015).
[73]F. Zhang, B. Gao, P. Zhou, and S. Pan, "Triangular pulse generation by polarization multiplexed optoelectronic oscillator," IEEE Photonics Technol. Lett. **28**, 1645–1648 (2016).
[74]T. Wu, Y. Jiang, C. Ma, Z. Jia, G. Bai, Y. Zi, and F. Huang, "Simultaneous triangular waveform signal and microwave signal generation based on dual-loop optoelectronic oscillator," IEEE Photonics J. **8**, 7805610 (2016).
[75]T. Hao, Q. Cen, Y. Dai, J. Tang, W. Li, J. Yao, N. Zhu, and M. Li, "Breaking the limitation of mode building time in an optoelectronic oscillator," Nat. Commun. **9**, 1839 (2018).
[76]T. Hao, J. Tang, W. Li, N. Zhu, and M. Li, "Tunable Fourier domain mode locked optoelectronic oscillator using stimulated Brillouin scattering," IEEE Photonics Technol. Lett. **30**(21), 1842–1845 (2018).
[77]T. Hao, J. Tang, W. Li, N. Zhu, and M. Li, "Fourier domain mode locked optoelectronic oscillator based on the deamplification of stimulated Brillouin scattering," OSA Continuum **1**(2), 408–415 (2018).
[78]T. Hao, J. Tang, W. Li, N. Zhu, and M. Li, "Harmonically Fourier domain mode-locked optoelectronic oscillator," IEEE Photonics Technol. Lett. **31**(6), 427–430 (2019).
[79]R. Liu *et al.*, "Generating ultra-wideband LFM waveforms with large time duration based on frequency-sweeping optoelectronic oscillation," in *18th International Conference on Optical Communications and Networks (ICOCN)* (IEEE, Huangshan, China, 2019), pp. 1–3.
[80]T. Hao, J. Tang, N. Shi, W. Li, N. Zhu, and M. Li, "Dual-chirp Fourier domain mode-locked optoelectronic oscillator," Opt. Lett. **44**(8), 1912–1915 (2019).
[81]L. Zhang *et al.*, "Frequency-sweep-range-reconfigurable complementary linearly chirped microwave waveform pair generation by using a Fourier domain mode locking optoelectronic oscillator based on stimulated Brillouin scattering," IEEE Photonics J. **12**(3), 5501010 (2020).
[82]Y. Li, T. Hao, G. Li, L. Wang, W. Li, Y. Dai, and M. Li, "Photonic generation of phase-coded microwave signals based on Fourier domain mode locking," IEEE Photonics Technol. Lett. **33**(9), 433–436 (2021).
[83]R. Liu *et al.*, "Simultaneous generation of ultra-wideband LFM and phase-coded LFM microwave waveforms based on an improved frequency-sweeping OEO," Opt. Commun. **459**, 124938 (2020).
[84]S. Zhu *et al.*, "Polarization manipulated Fourier domain mode-locked optoelectronic oscillator," J. Lightwave Technol. **38**(19), 5270–5277 (2020).
[85]Z. Zeng *et al.*, "Frequency-definable linearly chirped microwave waveform generation by a Fourier domain mode locking optoelectronic oscillator based on stimulated Brillouin scattering," Opt. Express **28**(9), 13861–13870 (2020).
[86]H. Zhang, F. Zhang, S. Pan, X. Ye, S. Liu, and H. Chen, "Photonic generation of linearly chirped microwave waveforms with tunable parameters," IEEE Photonics Technol. Lett. **32**(17), 1037–1040 (2020).
[87]P. Hao, H. Lu, R. Han, X. Wang, X. Liu, and X. S. Yao, "Fourier domain mode-locked opto-electronic oscillator with a diode-tuned bandpass filter," Opt. Express **28**(16), 23454–23466 (2020).
[88]Y. Wang, X. Li, J. Zhang, and J. Wo, "Spurious level and phase noise improved Fourier domain mode-locked optoelectronic oscillator based on a self-injection-locking technique," Opt. Express **29**, 7535–7543 (2021).
[89]X. Zhang, H. Zeng, J. Yang, Z. Yin, Q. Sun, and W. Li, "Novel RF-source-free reconfigurable microwave photonic radar," Opt. Express **28**(9), 13650–13661 (2020).
[90]T. Hao, J. Tang, W. Li, N. Zhu, and M. Li, "Microwave photonics frequency-to-time mapping based on a Fourier domain mode locked optoelectronic oscillator," Opt. Express **26**(26), 33582–33591 (2018).
[91]T. Hao, J. Tang, N. Shi, W. Li, N. Zhu, and M. Li, "Multiple-frequency measurement based on a Fourier domain mode-locked optoelectronic oscillator operating around oscillation threshold," Opt. Lett. **44**(12), 3062–3065 (2019).
[92]T. Hao, Q. Cen, S. Guan, W. Li, Y. Dai, N. Zhu, and M. Li, "Optoelectronic parametric oscillator," Light: Sci. Appl. **9**, 102 (2020).
[93]Y. K. Chembo, L. Larger, H. Tavernier, R. Bendoula, E. Rubiola, and P. Colet, "Dynamic instabilities of microwaves generated with optoelectronic oscillators," Opt. Lett. **32**(17), 2571–2573 (2007).
[94]Y. K. Chembo, L. Larger, and P. Colet, "Nonlinear dynamics and spectral stability of optoelectronic microwave oscillators," IEEE J. Quantum Electron. **44**, 858–866 (2008).
[95]M. Peil, M. Jacquot, Y. K. Chembo, L. Larger, and T. Erneux, "Routes to chaos and multiple time scale dynamics in broadband bandpass nonlinear delay electro-optic oscillators," Phys. Rev. E **79**, 026208-1–026208-15 (2009).
[96]L. Larger and J. M. Dudley, "Nonlinear dynamics: Optoelectronic chaos," Nature **465**, 41–42 (2010).
[97]K. E. Callan, L. Illing, Z. Gao, D. J. Gauthier, and E. Schöll, "Broadband chaos generated by an opto-electronic oscillator," Phys. Rev. Lett. **104**(11), 113901 (2010).
[98]J. Zheng *et al.*, "Spectral sculpting of chaotic-UWB signals using a dual-loop optoelectronic oscillator," IEEE Photonics Technol. Lett. **25**(24), 2397–2400 (2013).
[99]B. Romeira, F. Kong, J. M. L. Figueiredo, J. Javaloyes, and J. Yao, "High-speed spiking and bursting oscillations in a long-delayed broadband optoelectronic oscillator," J. Lightwave Technol. **33**, 503–510 (2015).
[100]J. H. T. Mbé, A. F. Talla, G. R. Chengui, A. Coillet, L. Larger, P. Woafo, and Y. K. Chembo, "Mixed-mode oscillations in slow-fast delayed optoelectronic systems," Phys. Rev. E **91**, 012902 (2015).
[101]J. H. T. Mbé, J. S. D. Kamaha, Y. K. Chembo, and P. Woafo, "Dynamics of wideband time-delayed optoelectronic oscillators with nonlinear filters," IEEE J. Quantum Electron. **55**(4), 5000106 (2019).
[102]G. R. G. Chengui, K. Jacques, P. Woafo, and Y. K. Chembo, "Nonlinear dynamics in an optoelectronic feedback delay oscillator with piecewise linear transfer functions from the laser diode and photodiode," Phys. Rev. E **102**, 042217 (2020).
[103]Z. Ge, T. Hao, J. Capmany, W. Li, N. Zhu, and M. Li, "Broadband random optoelectronic oscillator," Nat. Commun. **11**, 5724 (2020).
[104]J. Lasri *et al.*, "A self-starting hybrid optoelectronic oscillator generating ultra low jitter 10-GHz optical pulses and low phase noise electrical signals," IEEE Photonics Technol. Lett. **14**(7), 1004–1006 (2002).
[105]P. Devgan, D. Serkland, G. Keeler, K. Geib, and P. Kumar, "An optoelectronic oscillator using an 850-nm VCSEL for generating low jitter optical pulses," IEEE Photonics Technol. Lett. **18**(5), 685–687 (2006).
[106]Y. K. Chembo, A. Hmima, P.-A. Lacourt, L. Larger, and J. M. Dudley, "Generation of ultralow jitter optical pulses using optoelectronic oscillators with time-lens soliton-assisted compression," J. Lightwave Technol. **27**(22), 5160–5167 (2009).
[107]N. Huang, M. Li, Y. Deng, and N. H. Zhu, "Optical pulse generation based on an optoelectronic oscillator with cascaded nonlinear semiconductor optical amplifiers," IEEE Photonics J. **6**(1), 5500208 (2014).

[108]P. Zhou, F. Zhang, B. Gao, and S. Pan, "Optical pulse generation by an optoelectronic oscillator with optically injected semiconductor laser," IEEE Photonics Technol. Lett. **28**(17), 1827–1830 (2016).
[109]T. Sakamoto, T. Kawanishi, and M. Izutsu, "Optoelectronic oscillator using a $LiNbO_3$ phase modulator for self-oscillating frequency comb generation," Opt. Lett. **31**(6), 811–813 (2006).
[110]W. Li, W. T. Wang, W. H. Sun, L. Wang, J. G. Liu, and N. H. Zhu, "Generation of flat optical frequency comb using a single polarization modulator and a Brillouin-assisted power equalizer," IEEE Photonics J. **6**(2), 7900908 (2014).
[111]X. Xie *et al.*, "Low-noise and broadband optical frequency comb generation based on an optoelectronic oscillator," Opt. Lett. **39**(4), 785–788 (2014).
[112]Z. Xie *et al.*, "Tunable ultraflat optical frequency comb generator based on optoelectronic oscillator using dual-parallel Mach–Zehnder modulator," Opt. Eng. **56**(6), 066115 (2017).
[113]W. Zhang and J. Yao, "Silicon photonic integrated optoelectronic oscillator for frequency-tunable microwave generation," J. Lightwave Technol. **36**(19), 4655–4663 (2018).
[114]C. Gunn, D. Guckenberger, T. Pinguet *et al.*, "A low phase noise 10GHz optoelectronic RF oscillator implemented using CMOS photonics," in *Proceedings of the 54th IEEE International Solid-State Circuits Conference (ISSCC '07)* (IEEE, 2007), pp. 567–622.
[115]J. Tang, T. Hao, W. Li, D. Domenech, R. Baños, P. Muñoz, N. Zhu, J. Capmany, and M. Li, "Integrated optoelectronic oscillator," Opt. Express **26**(9), 12257–12265 (2018).
[116]T. Hao, J. Tang, D. Domenech, W. Li, N. Zhu, J. Capmany, and M. Li, "Toward monolithic integration of OEOs: From systems to chips," J. Lightwave Technol. **36**(19), 4565–4582 (2018).
[117]P. Salzenstein, H. Tavernier, K. Volyanskiy, N. N. T. Kim, L. Larger, and E. Rubiola, "Optical mini-disk resonator integrated into a compact optoelectronic oscillator," Acta Phys. Pol. **116**(4), 661–663 (2009).
[118]S. Srinivasan *et al.*, "Microwave generation using an integrated hybrid silicon mode-locked laser in a coupled optoelectronic oscillator configuration," in *CLEO: 2013* (IEEE, San Jose, CA, 2013).
[119]P. Primiani, F. Dijk, M. Lamponi, M. Chtioui, M. Vallet, M. Romanelli, and M. Alouini, "Tunable optoelectronic oscillator based on an integrated heterodyne source," in *IEEE International Topical Meeting on Microwave Photonics (MWP)* (IEEE, 2016), pp. 251–254.
[120]G. Chen, D. Lu, L. Guo, Q. Deng, W. Zhao, and L. Zhao, "An optoelectronic oscillator based on self-injection-locked monolithic integrated dual-mode amplified feedback laser," in *Asia Communications and Photonics Conference* (IEEE, 2017), p. Su2A-10.
[121]W. Zhang and J. P. Yao, "A silicon photonic integrated frequency-tunable optoelectronic oscillator," in *International Topical Meeting on Microwave Photonics (MWP)* (IEEE, Beijing, China, 2017), pp. 1–4.
[122]J. Tang, T. Hao, W. Li, D. Domenech, R. Banos, P. Munoz, N. Zhu, J. Capmany, and M. Li, "An integrated optoelectronic oscillator," in *International Topical Meeting on Microwave Photonics (MWP)* (IEEE, Beijing, China, 2017), pp. 1–4.
[123]J.-Y. Han *et al.*, "Wideband frequency-tunable optoelectronic oscillator with a directly modulated AlGaInAs/InP integrated twin-square microlaser," Opt. Express **26**, 31784–31793 (2018).
[124]Z. Xuan, L. Du, and F. Aflatouni, "Frequency locking of semiconductor lasers to RF oscillators using hybrid-integrated opto-electronic oscillators with dispersive delay lines," Opt. Express **27**(8), 10729–10737 (2019).
[125]X. Zhang *et al.*, "Simple frequency-tunable optoelectronic oscillator using integrated multi-section distributed feedback semiconductor laser," Opt. Express **27**(5), 7036–7046 (2019).
[126]M. Merklein *et al.*, "Widely tunable, low phase noise microwave source based on a photonic chip," Opt. Lett. **41**(20), 4633–4636 (2016).
[127]L. Nielsen and M. Heck, "A computationally efficient integrated coupled optoelectronic oscillator model," J. Lightwave Technol. **38**(19), 5430–5439 (2020).
[128]P. T. Do *et al.*, "Wideband tunable microwave signal generation in a silicon-micro-ring-based optoelectronic oscillator," Sci. Rep. **10**, 6982 (2020).
[129]X. Zou *et al.*, "Optoelectronic oscillators (OEOs) to sensing, measurement, and detection," IEEE J. Quantum Electron. **52**(1), 0601116 (2016).
[130]J. Yao, "Optoelectronic oscillators for high speed and high resolution optical sensing," J. Lightwave Technol. **35**(16), 3489–3497 (2017).
[131]L. D. Nguyen, K. Nakatani, and B. Journet, "Refractive index measurement by using an optoelectronic oscillator," IEEE Photonics Technol. Lett. **22**(12), 857–859 (2010).
[132]M. Li, W. Li, J. Yao, and J. Azaña, "Femtometer-resolution wavelength interrogation using an optoelectronic oscillator," in *Proceedings of IEEE Photonics Conference* (IEEE, Burlingame, CA, 2012), pp. 298–299.
[133]F. Kong, W. Li, and J. Yao, "Transverse load sensing based on a dual-frequency optoelectronic oscillator," Opt. Lett. **38**(14), 2611–2613 (2013).
[134]O. Okusaga *et al.*, "The OEO as an acoustic sensor," in *Proceedings of the Joint European Frequency and Time Forum and International Frequency Control Symposium* (IEEE, Prague, Czech Republic, 2013), pp. 66–68.
[135]T. Zhang, J. Zhu, T. Guo, J. Wang, and S. Ye, "Improving accuracy of distance measurements based on an optoelectronic oscillator by measuring variation of fiber delay," Appl. Opt. **52**(15), 3495–3499 (2013).
[136]C. H. Lee and S. H. Yim, "Optoelectronic oscillator for a measurement of acoustic velocity in acousto-optic device," Opt. Express **22**(11), 13634–13640 (2014).
[137]F. Kong, B. Romeira, J. Zhang, W. Li, and J. Yao, "A dual-wavelength fiber ring laser incorporating an injection-coupled optoelectronic oscillator and its application to transverse load sensing," J. Lightwave Technol. **32**(9), 1784–1793 (2014).
[138]Y. Zhu, X. Jin, H. Chi, S. Zheng, and X. Zhang, "High-sensitivity temperature sensor based on an optoelectronic oscillator," Appl. Opt. **53**(22), 5084–5087 (2014).
[139]S. Zhang, H. Chen, and H. Fu, "Fiber-optic temperature sensor using an optoelectronic oscillator," in *Proceedings of the 14th International Conference on Optical Communications and Networks (ICOCN)* (IEEE, 2015), pp. 1–3.
[140]Y. Wang, J. Zhang, and J. Yao, "An optoelectronic oscillator for high sensitivity temperature sensing," IEEE Photonics Technol. Lett. **28**(13), 1458–1461 (2016).
[141]S. Chew *et al.*, "Optoelectronic oscillator based sensor using an on-chip sensing probe," IEEE Photonics J. **9**(2), 5500809 (2017).
[142]Y. K. Chembo, "Machine learning based on reservoir computing with time-delayed optoelectronic and photonic systems," Chaos **30**(1), 013111 (2020).
[143]L. Larger, M. C. Soriano, D. Brunner, L. Appeltant, J. M. Gutierrez, L. Pesquera, C. R. Mirasso, and I. Fischer, "Photonic information processing beyond Turing: An optoelectronic implementation of reservoir computing," Opt. Express **20**, 3241–3249 (2012).
[144]Y. Paquot, F. Duport, A. Smerieri, J. Dambre, B. Schrauwen, M. Haelterman, and S. Massar, "Optoelectronic reservoir computing," Sci. Rep. **2**, 287 (2012).
[145]R. Martinenghi, S. Rybalko, M. Jacquot, Y. K. Chembo, and L. Larger, "Photonic nonlinear transient computing with multiple-delay wavelength dynamics," Phys. Rev. Lett. **108**, 244101 (2012).
[146]M. Hermans, P. Antonik, M. Haelterman, and S. Massar, "Embodiment of learning in electro-optical signal processors," Phys. Rev. Lett. **117**, 128301 (2016).
[147]L. Larger, A. Baylón-Fuentes, R. Martinenghi, V. S. Udaltsov, Y. K. Chembo, and M. Jacquot, "High-speed photonic reservoir computing using a time-delay-based architecture: Million words per second classification," Phys. Rev. X **7**, 011015 (2017).
[148]M. C. Soriano, S. Ortín, D. Brunner, L. Larger, C. R. Mirasso, I. Fischer, and L. Pesquera, "Optoelectronic reservoir computing: Tackling noise-induced performance degradation," Opt. Express **21**, 12–20 (2013).
[149]Y. Chen, L. Yi, J. Ke, Z. Yang, Y. Yang, L. Huang, Q. Zhuge, and W. Hu, "Reservoir computing system with double optoelectronic feedback loops," Opt. Express **27**, 27431–27440 (2019).
[150]F. Böhm, G. Verschaffelt, and G. Van der Sande, "A poor man's coherent Ising machine based on opto-electronic feedback systems for solving optimization problems," Nat. Commun. **10**, 3538 (2019).
[151]P. Devgan, "A review of optoelectronic oscillators for high speed signal processing applications," ISRN Electron. **2013**, 401969.
[152]M. Shin and P. Kumar, "Optical microwave frequency upconversion via a frequency-doubling optoelectronic oscillator," IEEE Photonics Technol. Lett. **19**, 1726–1728 (2007).

[153]B. Yang, X. Jin, Y. Chen, H. Chi, X. Zhang, S. Zheng, E. Tangdiongga, and T. Koonen, "Photonic microwave upconversion of vector signals based on an optoelectronic oscillator," IEEE Photonics Technol. Lett. **25**, 1758–1761 (2013).
[154]J.-Y. Lee, M.-S. Jeon, and J.-I. Song, "Remote optical frequency up-converter based on optoelectronic oscillator," IEEE Photonics Technol. Lett. **31**, 50–53 (2019).
[155]X. S. Yao and G. Lutes, "A high-speed photonic clock and carrier recovery device," IEEE Photonics Technol. Lett. **8**, 688–691 (1996).
[156]L. Huo, Y. Dong, C. Lou, and Y. Gao, "Clock extraction using an optoelectronic oscillator from high-speed NRZ signal and NRZ-to-RZ format transformation," IEEE Photonics Technol. Lett. **15**, 981–983 (2003).
[157]H. Tsuchida, "40-GHz subharmonic optical clock recovery using an injection-locked optoelectronic oscillator," Electron. Express **3**(15), 373–378 (2006).
[158]F. Cisternino, R. Girardi, S. Römisch, R. Calvani, E. Riccardi, and P. Garino, "A novel approach to pre-scaled clock recovery in OTDM systems," in *Proceedings of the European Conference on Optical Communication* (IEEE, Madrid, Spain, 1998), pp. 477–478.
[159]P. Devgan, "High speed signal processing using nonlinear fibers and opto-electronic devices," Ph.D. dissertation (Northwestern University, Evanston, IL, 2005).
[160]J. Lasri, P. Devgan, R. Tang, and P. Kumar, "Ultralow timing jitter 40-Gb/s clock recovery using a self-starting optoelectronic oscillator," IEEE Photonics Technol. Lett. **16**(1), 263–265 (2004).
[161]H. Tsuchida and M. Suzuki, "40-Gb/s optical clock recovery using an injection-locked optoelectronic oscillator," IEEE Photonics Technol. Lett. **17**(1), 211–213 (2005).
[162]H. Tsuchida, "Subharmonic optoelectronic oscillator," IEEE Photonics Technol. Lett. **20**(17), 1509–1511 (2008).
[163]S. Pan and J. Yao, "Optical clock recovery using a polarization modulator-based frequency-doubling optoelectronic oscillator," J. Lightwave Technol. **27**(16), 3531–3539 (2009).
[164]S. Pan and J. Yao, "Multichannel optical signal processing in NRZ systems based on a frequency-doubling optoelectronic oscillator," IEEE J. Sel. Top. Quantum Electron. **16**(5), 1460–1468 (2010).
[165]Q. Wang *et al.*, "Gaussian-like dual-wavelength prescaled clock recovery with simultaneous frequency-doubled clock recovery using an optoelectronic oscillator," Opt. Express **22**(3), 2798–2806 (2014).
[166]C. Lou, L. Huo, G. Chang, and Y. Z. Gao, "Experimental study of clock division using the optoelectronic oscillator," IEEE Photonics Technol. Lett. **14**, 1178–1180 (2002).
[167]Y. Xu, H. Peng, R. Guo, H. Du, Q. Yin, G. Hu, J. He, and Z. Chen, "Injection-locked millimeter wave frequency divider utilizing optoelectronic oscillator based optical frequency comb," IEEE Photonics J. **11**, 5501508 (2019).
[168]S. Liu, K. Lv, J. Fu, L. Wu, W. Pan, and S. Pan, "Wideband microwave frequency division based on an optoelectronic oscillator," IEEE Photonics Technol. Lett. **31**, 389–392 (2019).
[169]Y. Meng, T. Hao, W. Li, N. Zhu, and M. Li, "Microwave photonic injection locking frequency divider based on a tunable optoelectronic oscillator," Opt. Express **29**, 684–691 (2021).
[170]V. J. Urick, P. S. Devgan, J. D. McKinney, F. Bucholtz, and K. J. Williams, "Channelisation of radio-frequency signals using optoelectronic oscillator," Electron. Lett. **45**(24), 1242–1244 (2009).
[171]P. S. Devgan, M. W. Pruessner, V. J. Urick, and K. J. Williams, "Detecting low-power RF signals using a multimode optoelectronic oscillator and integrated optical filter," IEEE Photonics Technol. Lett. **22**(3), 152–154 (2010).
[172]Y. Shao, X. Han, M. Li, and M. Zhao, "RF signal detection by a tunable optoelectronic oscillator based on a PS-FBG," Opt. Lett. **43**(6), 1199–1202 (2018).
[173]G. Wang, T. Hao, W. Li, N. Zhu, and M. Li, "Detection of wideband low-power RF signals using a stimulated Brillouin scattering-based optoelectronic oscillator," Opt. Commun. **439**, 133–136 (2019).
[174]Z. Zhu *et al.*, "Highly sensitive broadband microwave frequency identification using a chip-based Brillouin optoelectronic oscillator," Opt. Express **27**(9), 12855–12868 (2019).
[175]Y. Shao *et al.*, "Low-power RF signal detection using a high-gain tunable OEO based on equivalent phase modulation," J. Lightwave Technol. **37**(21), 5370–5379 (2019).
[176]E. C. Levy, M. Horowitz, and C. R. Menyuk, "Modeling optoelectronic oscillators," J. Opt. Soc. Am. B **26**(1), 148–159 (2009).
[177]S. Pan and Y. Zhang, "Microwave photonic radars," J. Lightwave Technol. **38**(19), 5450–5484 (2020).
[178]R. Krishnan, A. Graell I Amat, T. Eriksson, and G. Colavolpe, "Constellation optimization in the presence of strong phase noise," IEEE Trans. Commun. **61**(12), 5056–5066 (2013).
[179]See http://www.klmicrowave.com for KandL Filter Data Sheet.
[180]M. Kaba, H.-W. Li, A. S. Daryoush, J.-P. Vilcot, D. Decoster, J. Chazelas, G. Bouwmans, Y. Quiquempois, and F. Deborgies, "Improving thermal stability of opto-electronic oscillators," IEEE Microwave Mag. **7**(4), 38 (2006).
[181]D. Eliyahu, K. Sariri, J. Taylor, and L. Maleki, "Optoelectronic oscillator with improved phase noise and frequency stability," Proc. SPIE **4998**, 139 (2003).
[182]Y. Zhang, D. Hou, and J. Zhao, "Long-term frequency stabilization of an opto-electronic oscillator using phase-locked loop," J. Lightwave Technol. **32**, 2408 (2014).
[183]D. Hou, X. P. Xie, Y. L. Zhang, J. T. Wu, Z. Y. Chen, and J. Y. Zhao, "Highly stable wideband microwave extraction by synchronizing widely tunable optoelectronic oscillator with optical frequency comb," Sci. Rep. **3**, 3509 (2013).
[184]W.-H. Tseng and K.-M. Feng, "Enhancing long-term stability of the optoelectronic oscillator with a probe-injected fiber delay monitoring mechanism," Opt. Express **20**, 1597 (2012).
[185]A. Bluestone, D. T. Spencer, S. Srinivasan, D. Guerra, J. E. Bowers, and L. Theogarajan, "An ultra-low phase-noise 20-GHz PLL utilizing an optoelectronic voltage-controlled oscillator," IEEE Trans. Microwave Theory Tech. **63**, 1046 (2015).
[186]H. Peng *et al.*, "Ultra-low phase noise and frequency agile X-band frequency synthesizer based on a phase locked optoelectronic oscillator," in *2019 Joint Conference of the IEEE International Frequency Control Symposium and European Frequency and Time Forum (EFTF/IFC)* (IEEE, 2019), pp. 1–3.
[187]W. Li, F. Kong, and J. Yao, "Arbitrary microwave waveform generation based on a tunable optoelectronic oscillator," J. Lightwave Technol. **31**(23), 3780–3786 (2013).
[188]W. Li and J. Yao, "Generation of linearly chirped microwave waveform with an increased time-bandwidth product based on a tunable optoelectronic oscillator and a recirculating phase modulation loop," J. Lightwave Technol. **32**(20), 3573–3579 (2014).
[189]Q. Cen, T. Hao, H. Ding, S. Guan, Z. Qin, K. Xu, Y. Dai, and M. Li, "Microwave photonic ising machine," arXiv:2011.00064 (2020).
[190]K. Ikeda, "Multiple-valued stationary state and its instability of the transmitted light by a ring cavity system," Opt. Commun. **30**, 257–261 (1979).
[191]A. Neyer and E. Voges, "High-frequency electro-optic oscillator using an integrated interferometer," Appl. Phys. Lett. **40**(1), 6–8 (1982).
[192]J.-P. Goedgebuer, L. Larger, and H. Porte, "Optical cryptosystem based on synchronization of hyperchaos generated by a delayed feedback tunable laser diode," Phys. Rev. Lett. **80**, 2249–2252 (1998).
[193]J.-P. Goedgebuer, P. Levy, L. Larger, C.-C. Chen, and W. T. Rhodes, "Optical communication with synchronized hyperchaos generated electrooptically," IEEE J. Quantum Electron. **38**, 1178–1183 (2002).
[194]M. W. Lee, L. Larger, and J. Goedgebuer, "Transmission system using chaotic delays between lightwaves," IEEE J. Quantum Electron. **39**, 931–935 (2003).
[195]A. Argyris *et al.*, "Chaos-based communications at high bit rates using commercial fibre-optic links," Nature **438**, 343–346 (2005).
[196]J. Ke, L. Yi, G. Xia, and W. Hu, "Chaotic optical communications over 100-km fiber transmission at 30-Gb/s bit rate," Opt. Lett. **43**, 1323–1326 (2018).
[197]T. E. Murphy *et al.*, "Complex dynamics and synchronization of delayed-feedback nonlinear oscillators," Philos. Trans. R. Soc., A **368**, 343–366 (2010).
[198]L. Illing, C. D. Panda, and L. Shareshian, "Isochronal chaos synchronization of delay-coupled optoelectronic oscillators," Phys. Rev. E **84**, 016213 (2011).
[199]X. Fang, B. Wetzel, J.-M. Merolla, J. M. Dudley, L. Larger, C. Guyeux, and J. M. Bahi, "Noise and chaos contributions in fast random bit sequence

generated from broadband optoelectronic entropy sources," IEEE Trans. Circuits Syst., I **61**, 888–901 (2014).
[200]W. Tian, L. Zhang, J. Ding, S. Shao, X. Fu, and L. Yang, "Ultrafast physical random bit generation from a chaotic oscillator with a silicon modulator," Opt. Lett. **43**, 4839–4842 (2018).
[201]F.-Y. Lin and J.-M. Liu, "Chaotic lidar," IEEE J. Sel. Top. Quantum Electron. **10**, 991–997 (2004).
[202]W.-T. Wu, Y.-H. Liao, and F.-Y. Lin, "Noise suppressions in synchronized chaos lidars," Opt. Express **18**, 26155–26162 (2010).
[203]J. Zheng, H. Wang, J. Fu, L. Wei, S. Pan, L. Wang, J. Liu, and N. Zhu, "Fiber-distributed ultra-wideband noise radar with steerable power spectrum and colorless base station," Opt. Express **22**, 4896–4907 (2014).
[204]T. Yao, D. Zhu, D. Ben, and S. Pan, "Distributed MIMO chaotic radar based on wavelength-division multiplexing technology," Opt. Lett. **40**, 1631–1634 (2015).
[205]Y. K. Chembo, "Laser-based optoelectronic generation of narrowband microwave chaos for radars and radio-communication scrambling," Opt. Lett. **42**, 3431–3434 (2017).
[206]S. Liu and A. Khope, "Latest advances in high-performance light sources and optical amplifiers on silicon," J. Semicond. **42**(4), 041307 (2021).
[207]X. Guo, A. He, and Y. Su, "Recent advances of heterogeneously integrated III–V laser on Si," J. Semicond. **40**(10), 101304 (2019).
[208]X. Zou, B. Lu, W. Pan, L. Yan, A. Stöhr, and J. Yao, "Photonics for microwave measurements," Laser Photonics Rev. **10**(5), 711–734 (2016).
[209]N. Shi, T. Hao, W. Li, and M. Li, "A compact multi-frequency measurement system based on an integrated frequency-scanning generator," Appl. Sci. **10**(23), 8571 (2020).
[210]S. Pan and J. Yao, "Photonics-based broadband microwave measurement," J. Lightwave Technol. **35**(16), 3498–3513 (2017).